Lithos 124 (2011) 82–102

Contents lists available at ScienceDirect

Lithos

journal homepage: www.elsevier.com/locate/lithos

Dating coeval mafic magmatism and ultrahigh temperature metamorphism in the Anápolis–Itauçu Complex, Central Brazil

Maria Emilia Schutesky Della Giustina [a,*], Márcio Martins Pimentel [a], Cesar Fonseca Ferreira Filho [a], Maria Helena Bezerra Maia de Hollanda [b]

[a] Universidade de Brasília, Instituto de Geociências, 70910-900, Brasília, DF, Brazil
[b] Universidade de São Paulo, Instituto de Geociências, Rua do Lago, 562, Cidade Universitária, 05508-900, São Paulo, SP, Brazil

ARTICLE INFO

Article history:
Received 19 January 2010
Accepted 5 November 2010
Available online 12 November 2010

Keywords:
Brasília Belt
Metamorphic zircon
UHT metamorphism
Layered mafic–ultramafic complexes
Hf-in-zircon
Coupled dissolution–reprecipitation process

ABSTRACT

Dating granulites has always been of great interest because they represent one of the most extreme settings of an orogen. Owing to the resilience of zircon, even in such severe environments, the link between *P–T* conditions and geological time is possible. However, a challenge to geochronologists is to define whether the growth of new zircon is related to pre- or post-*P–T* peak conditions and which processes might affect the (re) crystallization. In this context, the Anápolis–Itauçu Complex, a high-grade complex in central Brazil with ultrahigh temperature (UHT) granulites, may provide valuable information within this topic.

The Anápolis–Itauçu Complex (AIC) includes ortho- and paragranulites, locally presenting UHT mineral assemblages, with igneous zircon ages varying between 760 and 650 Ma and metamorphic overgrowths dated at around 650–640 Ma. Also common in the Anápolis–Itauçu Complex are layered mafic–ultramafic complexes metamorphosed under high-grade conditions.

This article presents the first geological and geochronological constraints of three of these layered complexes within the AIC, the Damolândia, Taquaral and Goianira–Trindade complexes. U–Pb (LA-MC-ICPMS, SHRIMP and ID-TIMS) zircon analyses reveal a spread of concordant ages spanning within an age interval of ~80 Ma with an "upper" intercept age of ~670 Ma. Under cathodoluminescence imaging, these crystals show partially preserved primary sector zoning, as well as internal textures typical of alteration during high-grade metamorphism, such as inward-moving boundaries. Zircon grains reveal homogeneous initial $^{176}Hf/^{177}Hf$ values in distinct crystal-scale domains in all samples. Moreover, Hf isotopic ratios show correlation neither with U–Pb ages nor with Th/U ratios, suggesting that zircon grains crystallized during a single growth event. It is suggested, therefore, that the observed spread of concordant U–Pb ages may be related to a memory effect due to coupled dissolution–reprecipitation process during high grade metamorphism.

Therefore, understanding the emplacement and metamorphism of this voluminous mafic magmatism is crucial as it may represent an additional heat source for the development of the ultrahigh temperature paragenesis recorded in the paragranulites.

1. Introduction

In recent years, petrological studies of granulite terranes have shown that these rocks can experience extreme *P–T* conditions, which may be substantially more vigorous than previously recognized. The so-called *ultrahigh temperature granulites* (UHT), recording temperatures higher than 900 °C in a moderate pressure environment, are present in most orogens. The origin of these rocks requires extremely hot crustal conditions, which cannot be explained even considering a large-hot orogen model, when compared to the real geological data there is still a thermal gap of about 100 to 200 °C which requires a supplementary heat source (Harley, 1998, 2004, 2008).

In central Brazil, such scenario may be recognized in the Anápolis–Itauçu Complex (AIC), which represents the metamorphic nucleus of the Brasilia Belt. The geological framework, with UHT paragenesis spatially associated with mafic granulites, suggests that this magmatism could represent an additional heat source to the development of the UHT metamorphic assemblages.

Previous studies combining geological and geochronological aspects of the UHT paragranulites of the AIC reveal the age of ~645 Ma for the peak of metamorphism (Baldwin and Brown, 2008; Moraes et al., 2002; Piuzana et al., 2003a). However, associated mafic complexes have never been the topic of such kind of research. The data available for the regional mafic magmatic event in the Brasilia Belt is limited to the arc terranes, exposed to the west of the AIC, and reveal crystallization ages of approximately 630 Ma (Hollanda et al., 2003; Laux et al., 2004).

Therefore, this study aims at describing the geology of three mafic–ultramafic complexes, occurring within the Anápolis–Itauçu Complex

* Corresponding author. Tel.: +55 61 3307 1113; fax: +55 61 3272 4286.
E-mail address: maria_emilia@unb.br (M.E.S.D. Giustina).

0024-4937
doi:10.1016/j.lithos.2010.11.004

and dating the emplacement and the high-grade metamorphic imprint of these layered bodies, as well as discuss their isotopic and geochronological record, in order to verify the relationship between mafic magmatism and the peak of metamorphism recorded in paragranulites of the AIC. Mafic intrusions emplaced into deep-crustal levels represent the most suitable rock association for this study. The intrusions investigated here partially record igneous textures, as well as the high-grade metamorphic imprint.

2. Geological setting

The Brasília Belt is a Neoproterozoic orogen in central Brazil, developed throughout island arc amalgamation and continental collision between the São Francisco Craton and the Paranapanema block to the south, which is covered by the Paraná Basin (Fig. 1; Pimentel et al., 2000; Valeriano et al., 2008). It is part of a global network of Neoproterozoic orogenic belts, which resulted in the final amalgamation of Gondwana. It may be divided into four domains: (i) in the easternmost part is a thrust-and-fold belt consisting of various Neoproterozoic metasedimentary sequences formed along the western margin of the São Francisco Craton, (ii) in the central part of the belt, the metamorphic core is exposed, comprising high-grade rocks and ultrahigh temperature granulites — the Anápolis–Itauçu Complex, (iii) the Goiás Massif, interpreted as a microcontinent/exotic terrane accreted to the orogen at the end of the Neoproterozoic, and (iv) the Goiás Magmatic Arc, which represents a juvenile terrane forming the westernmost part of the belt (Brito Neves and Cordani, 1991; Fuck et al., 1994; Pimentel et al., 2000; Pimentel and Fuck, 1992; Fig. 1A).

The Anápolis–Itauçu Complex (AIC) is located in the southern branch of the Brasília Belt (Fig. 1B). It constitutes an elongated NW–SE zone of high-grade rocks exposed between the Goiás Magmatic Arc and lower-grade metasediments of the Neoproterozoic Araxá Group, representing a fore-arc ophiolitic mélange (Piuzana et al., 2003b). Geological contacts are marked by high-angle shear-zones in the northern segment of the AIC and by low-angle nappe structures in its meridional exposure, thus preventing the identification of clear stratigraphic or cross-cutting relationships between the different rock units. However, geochronological data support the interpretation that at least part of the AIC may represent high-grade equivalents of the Araxá Group (Piuzana et al., 2003b) and, moreover, it might be an exposure of the root of the original mountain chain.

The AIC includes a variety of rock types forming NW-oriented segment, in which three main rock associations may be recognized: i) orthogranulites; ii) paragranulites; and iii) granites (Fig. 1B).

The orthogranulites are represented by tonalitic to granodioritic gneisses, as well as by mafic rocks, exposed either as dioritic/gabbroic granulites or as mafic–ultramafic complexes. Such layered bodies are composed of peridotite, pyroxenite, gabbro and gabbro-anorthosite. Relict igneous textures and layering are usually observed. However, these complexes are often strongly foliated and metamorphosed under amphibolite to granulite facies conditions (Nilson, 1992; Silva, 1997). Geochemical analysis point toward a tholeiitic parental magma, with LREE enrichment and a negative Eu anomaly, and the high-Al content of relict igneous pyroxenes suggests that the intrusion took place at deep levels in the crust (Nilson, 1992; Silva, 1991, 1997).

Example of these layered bodies are the Damolândia, Taquaral (Silva, 1997), Goianira–Trindade (Nilson and Motta, 1969) and Águas Claras complexes (Nilson, 1992), which are interpreted to be coeval with those exposed to the west, within the Goiás Magmatic Arc domain (Laux et al., 2004).

Paragranulitesare typically represented by aluminous granulites with variable amounts of sillimanite, garnet, spinel, cordierite and feldspars. These rocks occur either as massive outcrops or form bands in stromatic migmatites, in which fine-grained mafic granulites interpreted as metabasalts are also observed (Winge, 1995). Calc-silicate rocks and impure quartzites are also recognized. Ultrahigh temperature mineral assemblages, such as saphirine + quartz, orthopyroxene + sillimanite + quartz, wollastonite + scapolite and hercynite + quartz have been identified in several localities of the AIC and revealed temperatures higher than 1100 °C, at moderate pressures (~10 kbar; Baldwin et al., 2005; Moraes et al., 2002, 2007). The paragranulites preserve composite *P–T* paths, with a first near-isothermal decompressional phase when the thermal peak is achieved, followed by a near-isobaric cooling stage (Baldwin and Brown, 2008; Moraes et al., 2002).

A large number of granites also constitute the AIC (Fig. 1B). They show variable deformational and metamorphic overprint, achieving even granulite facies conditions (Piuzana et al., 2003a). Most of these granitic rocks are peraluminous and the Nd isotopic signature indicates that they may be the melting products of either the aluminous paragranulites of the AIC or metasedimentary rocks of the Araxá Group (Piuzana et al., 2003a). U–Pb zircon ages for cores and metamorphic rims are identical in some of these bodies and, therefore, the granites are interpreted as deep-crustal, syn-tectonic intrusions (Piuzana et al., 2003a).

SHRIMP U–Pb ages of igneous zircon from felsic orthogranulites vary between 760 and 650 Ma and metamorphic overgrowths are dated at 650–640 Ma (Piuzana et al., 2003a). T_{DM} Sm–Nd model ages of orthogranulites fall into two age intervals, between 2.3–1.9 Ga and 1.7–1.4 Ga, and ε_{Nd} (T) values are negative, ranging from −9.3 to −1.4 (Piuzana et al., 2003a). The younger T_{DM} values are in agreement with zircon inheritance pattern observed in paragranulites (2.0 to 0.8 Ga; Piuzana et al., 2003a), which indicates that the Neoproterozoic Goiás Magmatic Arc, exposed to the west, might have been one of the sedimentary sources contributing to the basin (Piuzana et al., 2003a).

3. Methods

3.1. Whole-rock analyses

The reported major and minor elements analyses (MgO, CaO, K_2O, Ti, and Cr) for drill cores of the Damolândia and Taquaral layered intrusions are part of the exploration database of the International Nickel Venture. Drill core analyses were performed on samples representative of 1-meter intervals throughout drill holes and were carried on by SGS GEOSOL LABORATORIES LTDA (Belo Horizonte-MG) using an inductively coupled plasma atomic emission spectrometer (ICP-AES).

Sm–Nd isotopic analyses followed the method described by Gioia and Pimentel (2000) and were carried out at the Geochronology Laboratory of the University of Brasília. Whole rock powders (ca. 50 mg) were mixed with ^{149}Sm–^{150}Nd spike solution and dissolved in Savillex capsules. Sm and Nd extraction of whole-rock samples followed conventional cation exchange techniques. Sm and Nd samples were loaded on Re evaporation filaments of double filament assemblies and the isotopic measurements were carried out on a multi-collector Finnigan MAT 262 mass spectrometer in static mode. Uncertainties for Sm/Nd and $^{143}Nd/^{144}Nd$ ratios are better than ±0.5% (2σ) and ±0.005% (2σ), respectively, based on repeated analyses of international rock standards BHVO-1 and BCR-1. The $^{143}Nd/^{144}Nd$ ratios were normalized to $^{146}Nd/^{144}Nd$ of 0.7219 and the decay constant used was 6.54×10^{-12} a^{-1}. The T_{DM} values were calculated using the model of DePaolo (1981). Nd procedure blanks were better than 100 pg.

3.2. In situ zircon analyses

Zircon concentrates were extracted using conventional gravimetric and magnetic separation techniques at the Geochronology Laboratory of the University of Brasília. Zircon grains were selected under a binocular microscope to obtain fractions of similar size, shape and color. For in situ U–Pb and Hf analyses, hand-picked zircon grains were mounted in epoxy blocks and polished to obtain a smooth

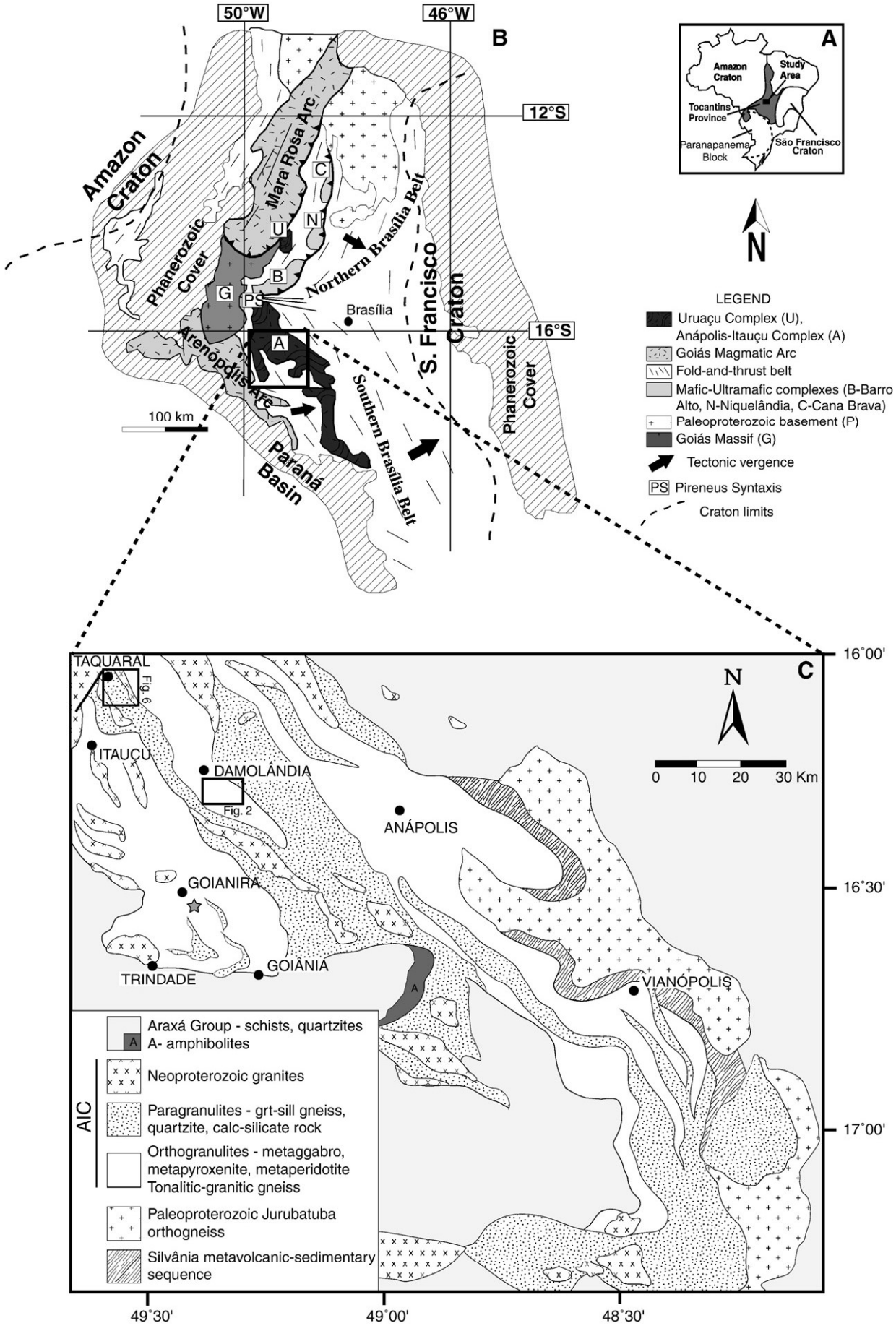
50°W
46°W
B
12°S
16°S
Amazon Craton
Phanerozoic Cover
Mara Rosa Arc
Northern Brasília Belt
S. Francisco Craton
Phanerozoic Cover
Arenópolis Arc
Southern Brasília Belt
Paraná Basin
Brasília
C
U
N
B
G
PS
A
100 km
A
Amazon Craton
Study Area
Tocantins Province
Paranapanema Block
São Francisco Craton
N
LEGEND
Uruaçu Complex (U), Anápolis-Itauçu Complex (A)
Goiás Magmatic Arc
Fold-and-thrust belt
Mafic-Ultramafic complexes (B-Barro Alto, N-Niquelândia, C-Cana Brava)
Paleoproterozoic basement (P)
Goiás Massif (G)
Tectonic vergence
PS Pireneus Syntaxis
Craton limits
TAQUARAL
Fig. 6
ITAUÇU
DAMOLÂNDIA
Fig. 2
ANÁPOLIS
GOIANIRA
TRINDADE
GOIÂNIA
VIANÓPOLIS
A
C
N
0 10 20 30 Km
16°00'
16°30'
17°00'
49°30'
49°00'
48°30'
Araxá Group - schists, quartzites
A- amphibolites
AIC
Neoproterozoic granites
Paragranulites - grt-sill gneiss, quartzite, calc-silicate rock
Orthogranulites - metaggabro, metapyroxenite, metaperidotite
Tonalitic-granitic gneiss
Paleoproterozoic Jurubatuba orthogneiss
Silvânia metavolcanic-sedimentary sequence

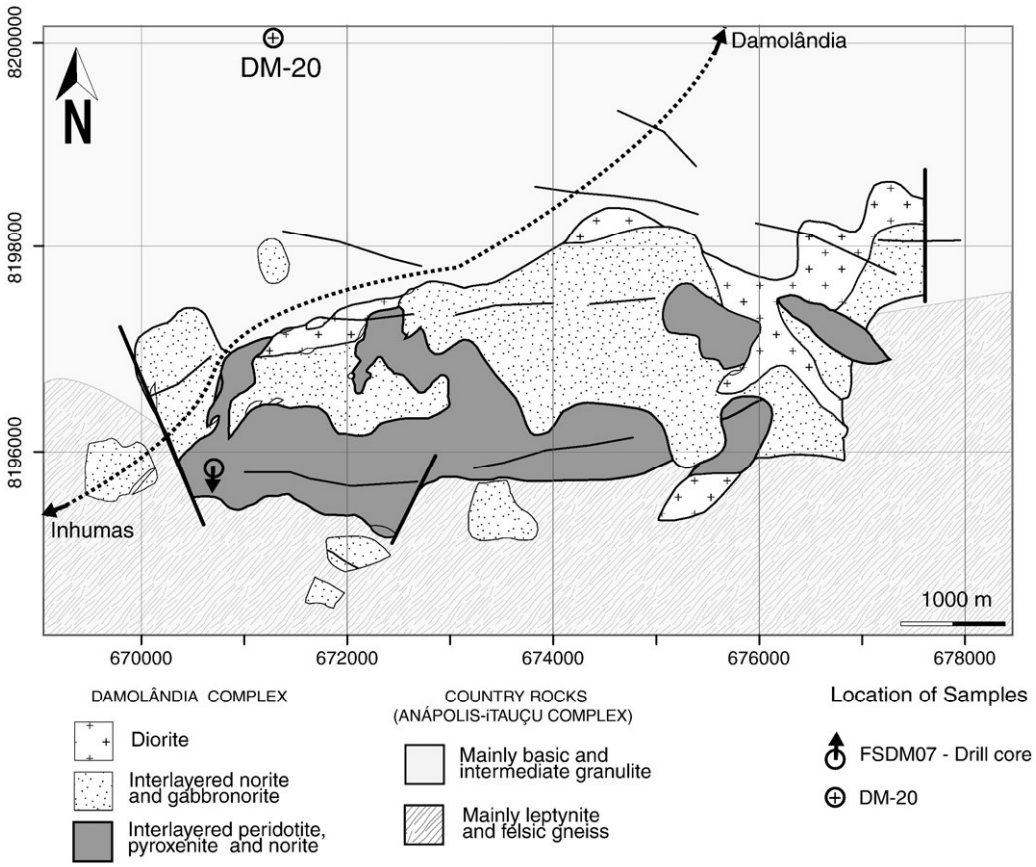

Fig. 2. Geology of the Damolândia Complex (from unpublished report of International Nickel Venture Ltd.; UTM coordinate system, datum SAD-69, zone 22).

surface. Backscattered electron and cathodoluminescence images were obtained in order to investigate the internal structures of the zircon crystals prior to analysis. Cathodoluminescence images were obtained using a LEO-1430 electronic microscope at the University of Pará (UFPA) working at 10 kV. Before LA-MC-ICPMS analyses, mounts were cleaned with dilute (ca. 2%) HNO_3. The samples were mounted in an in-house specially designed laser cell and loaded into a New Wave UP213 Nd:YAG laser ($\lambda = 213$ nm), linked to a Thermo Finnigan Neptune Multi-collector ICPMS. Helium was used as the carrier gas and mixed with argon before entering the ICP. The laser was run at a frequency of 10 Hz and energy of ~100 mJ/cm^2 with a spot of 30 μm for U–Pb dating and 40 μm for Hf isotopic analyses.

The U–Pb and Hf LA-MC-ICPMS analyses were performed at the Geochronology Laboratory of the University of Brasília and followed the analytical procedure described by Bühn et al. (2009) and Matteini et al. (2010), respectively.

Two international zircon standards were analyzed throughout the U–Pb LA-MC-ICPMS analyses. Zircon GJ-1 reference material (RM) (Jackson et al., 2004) was used as the primary reference material in a standard-sample bracketing method, accounting for mass-bias and drift correction. The resulting correction factor for each sample analysis considers the relative position of each analysis within the sequence of 4 samples bracketed by two RM and two blank analyses each (Albarède et al., 2004). The Temora 2 RM (Black et al., 2004) was run at the start and at the end of each analytical session, yielding accuracy around 2% and a precision in the range of 1% (1σ). The errors of samples analyses were propagated by quadratic addition of reproducibility observed for the GJ-1 RM and within-run precision of each unknown analysis. Zircon grains with $^{206}Pb/^{204}Pb$ lower than 1000 were rejected. Plotting of U–Pb data and age calculations were performed using ISOPLOT version 3.0 (Ludwig, 2003) and errors for isotopic ratios are presented at the 1σ level.

Hf isotopic measurements were carried out on zircon grains previously analyzed for U–Pb. Only U–Pb concordant grains (±5%) were selected. The Hf spot analyses were located in the same CL region of zircon grains and, whenever possible, just on top of the U–Pb analytical pit. Before the laser ablation analyses, JMC 475 10 ppb standard solution, doped with Yb (Yb/Hf = 0.02), was run, yielding a mean $^{176}Hf/^{177}Hf$ ratio of 0.282171 ± 20 ($n = 4$) which is in agreement with values reported in the literature (e.g. 0.282163 ± 09; Blichert-Toft et al. (1997); 0.282162 ± 24; Chu et al. (2002)). During in situ analytical session, GJ-1 zircon (Jackson et al., 2004) was monitored as a reference material and provided an average $^{176}Hf/^{177}Hf$ value of 0.282001 ± 21 ($n = 10$) in agreement with Zeh et al. (2007; 0.282003 ± 15), Morel et al. (2008; 0.282000 ± 05) and Xie et al. (2008; 0.282028 ± 34). The mass-bias correction considered the signal of ^{171}Yb and ^{173}Yb and, additionally, these isotopes, as well as ^{175}Lu, were applied in the isobaric interference correction of Yb and Lu on the ^{176}Hf signal (Matteini et al., (2010)). The studied zircon grains show very low Lu/Hf values (<0.0004), which reflect that the primary Hf isotopic composition is preserved and, consequently, no over-correction is needed. Calculation of ε_{Hf} and T_{DM} model ages for each single spot analyses were based on the $^{206}Pb/^{238}U$ age, previously determined in the same grain. Errors for isotopic ratios are presented at the 2σ level.

Fig. 1. A) Tectonic sketch map of the Tocantins Province, central Brazil. B) Regional sketch map of the Brasilia Belt, in the eastern part of the Tocantins Province (modified from Giustina et al., 2009). C) Geological map of the central part of the Anápolis–Itauçu Complex (modified from Piuzana et al., 2003a). The star represents the location of sample INHO-01.

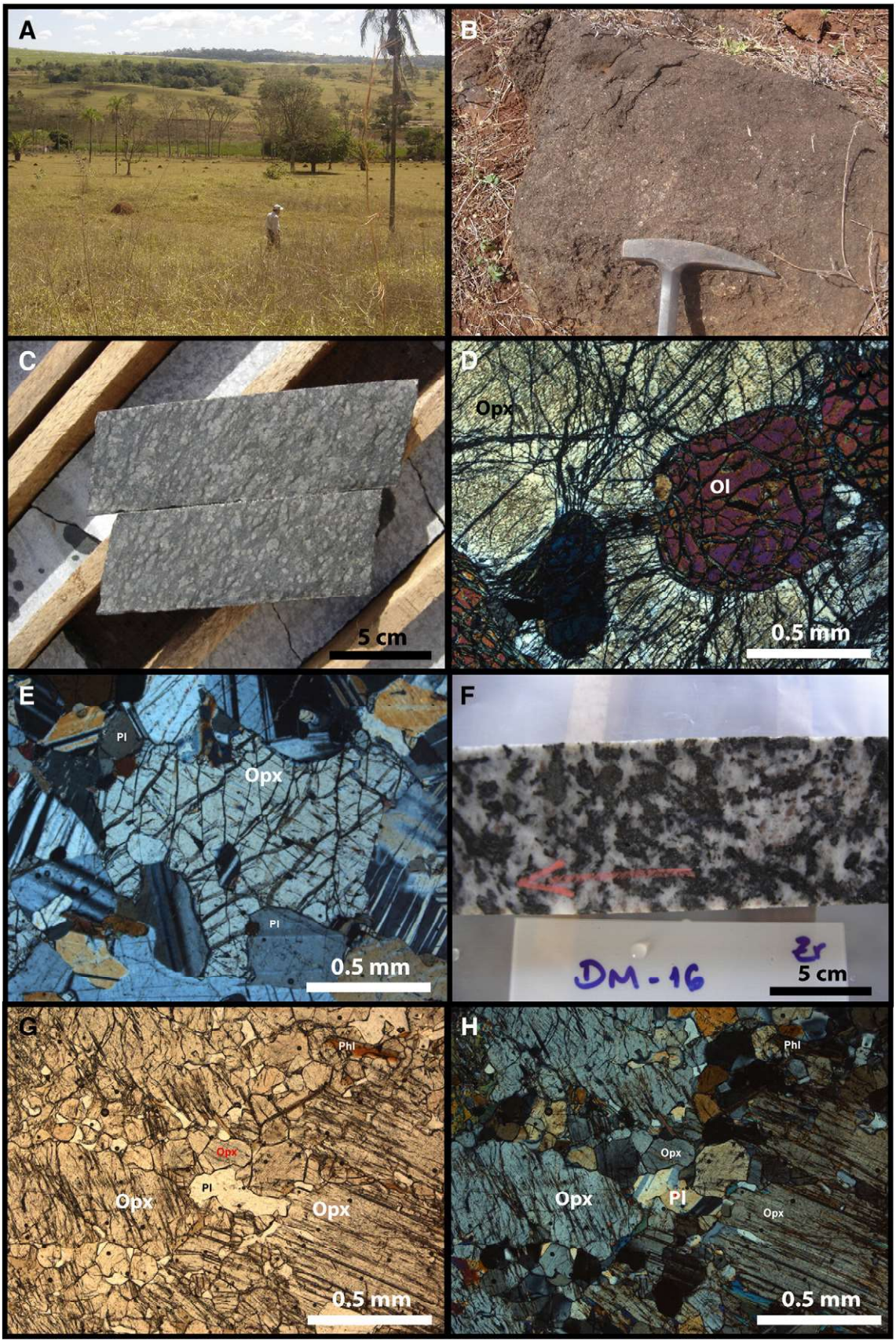

Fig. 3. A) View of the area close to the drill core FSDM-07. Rare outcrops and abundant dark brownish termite mounts developed on soil from ultramafic rocks. B) Orthopyroxenite with interstitial white plagioclase. C) Harzburgite from drill hole FSDM-07. D) Photomicrograph of harzburgite consisting of cumulus olivine (Ol) enclosed in large orthopyroxene oikocryst (Opx). E) Photomicrograph of norite consisting of cumulus orthopyroxene (Opx) and plagioclase (Pl). F) Zircon-bearing hornblende gabbronorite. Sample DM-16 from drill hole FSDM-07. G) and H) Photomicrograph of partially recrystallized plagioclase-bearing orthopyroxene. Large igneous orthopyroxene crystals are recrystallized into fine-grained granoblastic aggregates.

Ion microprobe analyses were carried out in one sample using SHRIMP I at the Research School of Earth Sciences, Australian National University, Canberra, Australia. Data were collected and reduced as described by Williams and Claesson (1987) and Compston et al. (1992). Uncertainties are given at 1σ level, and ages are quoted at 95% confidence level. Reduction of raw data was carried out using Squid 1.02 (Ludwig, 2001). U/Pb isotopic ratios were referenced to the RSES standard zircon AS3 (1099 Ma, $^{*206}Pb/^{238}U = 0.1859$, Paces and Miller (1993). U and Th concentrations were determined relative to those measured in the RSES standard SL13.

3.3. Zircon U–Pb ID-TIMS analyses

For the conventional U–Pb analyses, zircon fractions were dissolved in concentrated HF and HNO_3 ($HF:HNO_3 = 4:1$) using microcapsules in Parr-type bombs. A mixed ^{205}Pb–^{235}U spike was used. Chemical extraction followed standard anion exchange technique, using Teflon microcolumns, following modified procedures from Krogh (1973). Pb and U were loaded together on single Re filaments with H_3PO_4 and Si gel, and isotopic analyses were carried out on a Finnigan MAT-262 multi-collector mass spectrometer equipped with secondary electron multiplier-ion counting, at the Geochronology Laboratory of the University of Brasília. Procedure blanks for Pb, at the time of analyses, were better than 20 pg. Data reduction and age calculations were performed using the PBDAT (Ludwig, 1993) and ISOPLOT version 3.0 (Ludwig, 2003) software. Errors for isotopic ratios are quoted at 2σ.

4. Results

4.1. Damolândia and Taquaral layered complexes

The Damolândia and Taquaral layered mafic–ultramafic complexes (Fig. 1B) occurs within high-grade gneiss and granulites of the AIC. Both layered complexes were overprinted by heterogeneous high-grade metamorphism and associated tectonism. While primary igneous textures and mineralogy are largely preserved in rocks of the EW trending Damolândia Complex (Fig. 2), such features are just locally preserved in the NNW trending Taquaral Complex (Fig. 6), which consists mainly of highly foliated and recrystallized mafic–ultramafic rocks.

4.1.1. Damolândia

The Damolândia Complex is a poorly exposed medium-size (ca 15 km^2) layered intrusion. Extensive mapping and mineral exploration data carried out by International Nickel Venture Ltd. in 2006–2008 provided constraints on the geology and stratigraphy of the layered sequence (Fig. 2). The host rocks of the Damolândia Complex were not investigated in detail, but regional mapping indicates that they consist mainly of basic to intermediate granulite in the north, and highly foliated leptynite[1] and felsic gneiss in the south (Fig. 2). Mafic–ultramafic rocks of the Damolândia Complex form irregular domains of interlayered peridotite–pyroxenite–norite associated with domains of mafic rocks, mainly norite and gabbronorite, and domains where medium to coarse-grained diorite occur. Layered rocks of the Damolândia Complex are heterogeneously tectonized and recrystallized in discrete zones, where primary igneous rocks were transformed into highly foliated mafic or ultramafic granulites. Due to poor exposure of mafic and ultramafic rocks, the mapped domains are based on soil characteristics (Fig. 3A) supported by scattered outcrops (Fig. 3B) and soil geochemistry surveys.

[1] Leptynites are fine-grained leucocratic sill-grt gneisses with a granoblastic texture, probably of granitic nature (Winge and Danni, 1994).

Extensive drilling developed in the southwestern portion of the Damolândia Complex expose complete sections of the interlayered peridotite–pyroxenite–norite domain. A representative drill core from this domain consists of a ca 200 meter-thick sequence of ultramafic cumulates within mafic cumulates (FSDM07; Fig. 4). The layered sequence in the core is not constrained by primary structures, but is defined by aligned prismatic pyroxenes indicating steep dip to the north. Norite and gabbronorite are orthopyroxene and plagioclase cumulates, with variable amounts of intercumulus clinopyroxene, hornblende and minor phlogopite. Pyroxenite consists of cumulus orthopyroxene, or orthopyroxene and chromite (ca 1–3 vol.%), with variable amounts of intercumulus plagioclase, clinopyroxene, hornblende and minor phlogopite. Textures of pyroxenite vary from medium- to coarse-grained adcumulate (orthopyroxenite), to mesocumulate and orthocumulates (usually websterite or melanorite). The transition from pyroxenite to norite is gradational and characterized by the increase of interstitial plagioclase. Cyclic interlayering of peridotite (mainly harzburgite) and pyroxenite characterizes the central zone of ultramafic cumulates in drill hole FSDM-07 (Fig. 4). Peridotite (Fig. 3C and D) is an olivine and chromite (ca 1–3 vol.%) cumulate with variable amounts of intercumulus orthopyroxene and minor clinopyroxene, hornblende, plagioclase and phlogopite. Interlayered olivine-rich peridotite (MgO>27 wt.%) and pyroxenite (MgO<17 wt.%) form up to dozen meter-thick layers with sharp contacts. Few cross-cutting bodies of coarse-grained hornblende-bearing gabbronorite or hornblende diorite (Fig. 3F) occur throughout the layered sequence. These bodies are usually few meter-thick and have accessory ilmenite, apatite and zircon, suggesting the crystallization from evolved magmas possibly resulting from residual trapped liquids.

Cumulus minerals in the layered rocks suggest that the sequence of crystallization in the Damolândia Complex consists of olivine + chromite, orthopyroxene + chromite, orthopyroxene, orthopyroxene + plagioclase and orthopyroxe + plagioclase + clinopyroxene. The crystallization sequence described for the Damolândia Complex is very common in mafic–ultramafic intrusions (e.g. Bushveld Complex — Cameron, 1978; Serra da Onça; Ferreira Filho et al., 2007). The correlation of MgO content with CaO, TiO_2, K_2O and Cr for layered rocks of the drill hole FSDM-07 (Fig. 5) corresponds to this sequence of crystallization of cumulus minerals. High MgO contents of peridotite samples (up to 41 wt.%) suggests high MgO content of olivine. Low CaO and TiO_2 contents are consistent with the predominance of orthopyroxene over clinopyroxene in the layered rocks, while high Cr contents are consistent with the presence of chromite in both peridotite and pyroxenite samples. Scattered high contents of K_2O are associated with disseminated interstitial phlogopite. High K_2O contents show no correlation with MgO content, suggesting that they result from inhomogeneous assimilation of crustal rocks by the parental magma.

Primary igneous texture and mineralogy prevail throughout the layered sequence of the drill hole FSDM-07. Recrystallization and ductile deformation are restricted to few meter-wide discrete zones. In these zones the primary igneous mineralogy is partially (Fig. 3G and H) to completely recrystallized into fine-grained granoblastic assemblages of metamorphic minerals. Recrystallized norite and gabbronorite consist of fine-grained granoblastic aggregates of plagioclase, orthopyroxene, clinopyroxene and dark-brown amphibole. This assemblage indicates that recrystallization occurred under conditions of high temperature (equivalent to the granulite facies of regional metamorphism).

4.1.2. Taquaral

The Taquaral Complex (Fig. 6) was considered by Silva (1997) as a large (up to 50 km-long) layered mafic–ultramafic complex subjected to high-grade metamorphism and associated tectonism. Silva (1997) proposed a stratigraphic column with 5 km of inferred thickness for the Taquaral Complex. However, extensive exploration carried out by

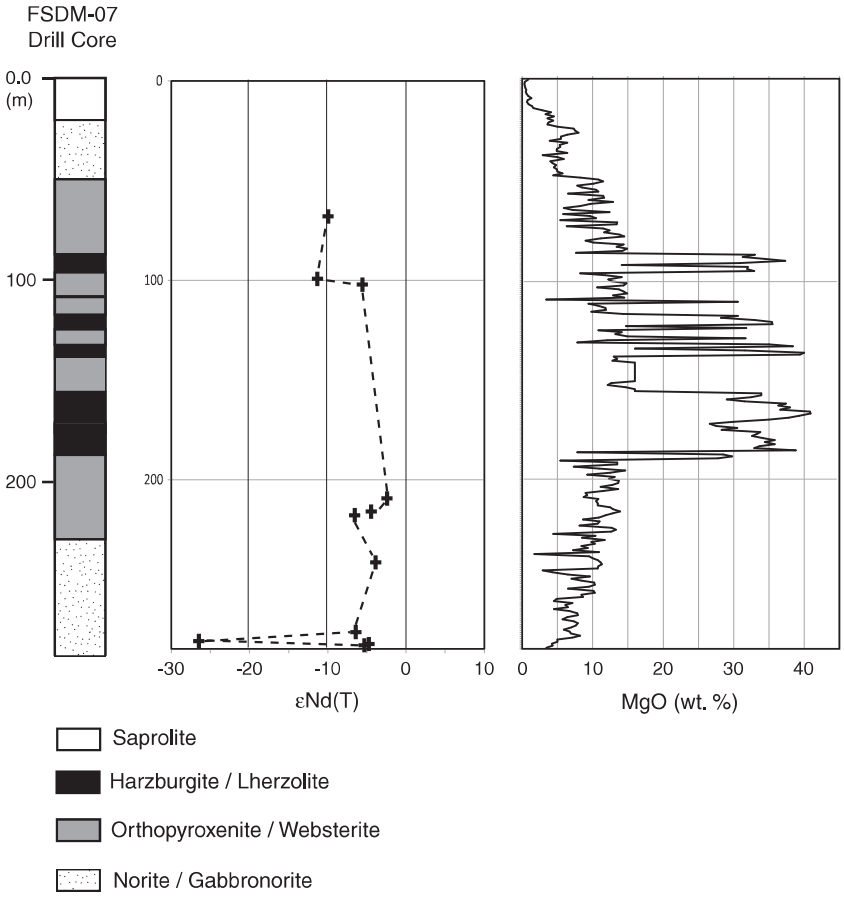

Fig. 4. Log, $\varepsilon_{Nd(T)}$ and MgO content for drill core FSDM-07 in Damolândia Complex (see Fig. 2 for location).

mining companies in the Taquaral Complex indicates that it consists of several elongated small to medium-size (up to 15 km-long) highly tectonized mafic and mafic–ultramafic bodies. Stratigraphic correlations between these different bodies are unconstrained and the Taquaral Complex should be considered as a cluster of NNW trending mafic and mafic–ultramafic lenses. Detailed mapping supported by exploration data was developed by International Nickel Venture (INV) Ltd. in 2007–2008 in the northern segment of the Taquaral Complex. Results indicate the existence of several small to medium-size mafic–ultramafic bodies (Fig. 6) surrounded by high-grade felsic gneiss and leptynite. Mapped mafic and ultramafic rocks of the Taquaral Complex are highly tectonized and recrystallized. They have pervasive tectonic foliation (Fig. 7A and B) parallel with the NNW (subvertical to SW dip) trend of host rocks.

Limited drilling developed by INV Ltd. exposed complete sections of interlayered peridotite, pyroxenite and gabbronorite. A representative drill core (FSTQ-01, see location in Fig. 6) from the mapped mafic–ultramafic rocks consists of a ca 60 meter-thick sequence of mainly peridotite at the base of the core, followed by a ca 100 meter-thick sequence of interlayered pyroxenite and gabbronorite rocks (Fig. 8). The upper part of the core consists mainly of silimanite–garnet leptynite tectonically imbricated with mafic rocks. Mafic and ultramafic rocks have mainly tectonic fabric consisting of foliated fine-grained granoblastic aggregates. Primary cumulate textures, preserved in several few-meter thick zones throughout the drill core, allow the recognition of primary igneous mineralogy and textures. Peridotite (Fig. 7B, C and D) is a medium- to coarse-grained olivine and chromite (ca 1–3 vol.%) cumulate with variable amounts of intercumulus clinopyroxene, orthopyroxene and minor brownish hornblende and phlogopite. Peridotite predominate at the base of the core interlayered with thin (usually less than 1–2 meter-thick) pyroxenite layers. Pyroxenite (Fig. 7E and F) consists of cumulus orthopyroxene or orthopyroxene and clinopyroxene, with variable amounts of intercumulus plagioclase, hornblende and minor phlogopite. Textures of pyroxenite vary from medium- to coarse-grained adcumulate (orthopyroxenite or websterite), to mesocumulate and orthocumulates (usually melagabbronorite). Pyroxenite occurs interlayered with rare thin peridotite layers within a zone where mafic rocks prevail. Interlayered peridotite and pyroxenite become less abundant toward the upper zone of the drill hole, suggesting progressive fractionation within the layered sequence. Restricted zones where mafic rocks have primary igneous fabric indicate that they consist mainly of medium-grained gabbronorite (orthopyroxene + clinopyroxene + plagioclase cumulate) and ilmenite gabbronorite (Fig. 7G). Gabbronorite has variable amounts of intercumulus hornblende and phlogopite. A 50 centimeter-thick zone of coarse-grained anisotropic metadiorite interlayered with gabbronorite and pyroxenite was sampled for geochronological studies (sample TQ-14). This sample consists mainly of plagioclase and pyroxene replaced by hornblende, with accessory apatite (ca 1 vol.%) and zircon.

Cumulus minerals in the layered rocks suggest that the sequence of crystallization in the FSTQ-01 drill core consists of olivine + chromite, orthopyroxene + chromite, orthopyroxene + clinopyroxene, orthopyroxene + clinopyroxene + plagioclase and orthopyroxene + clinopyroxene + plagioclase + ilmenite. This crystallization sequence is different from the Damolândia Complex, indicating an early crystallization of clinopyroxene in the Taquaral Complex. The crystallization sequence described for the Taquaral Complex is similar to the Great Dyke (Wilson, 1982) and the Niquelândia Layered Complex (Ferreira Filho et al., 2010).

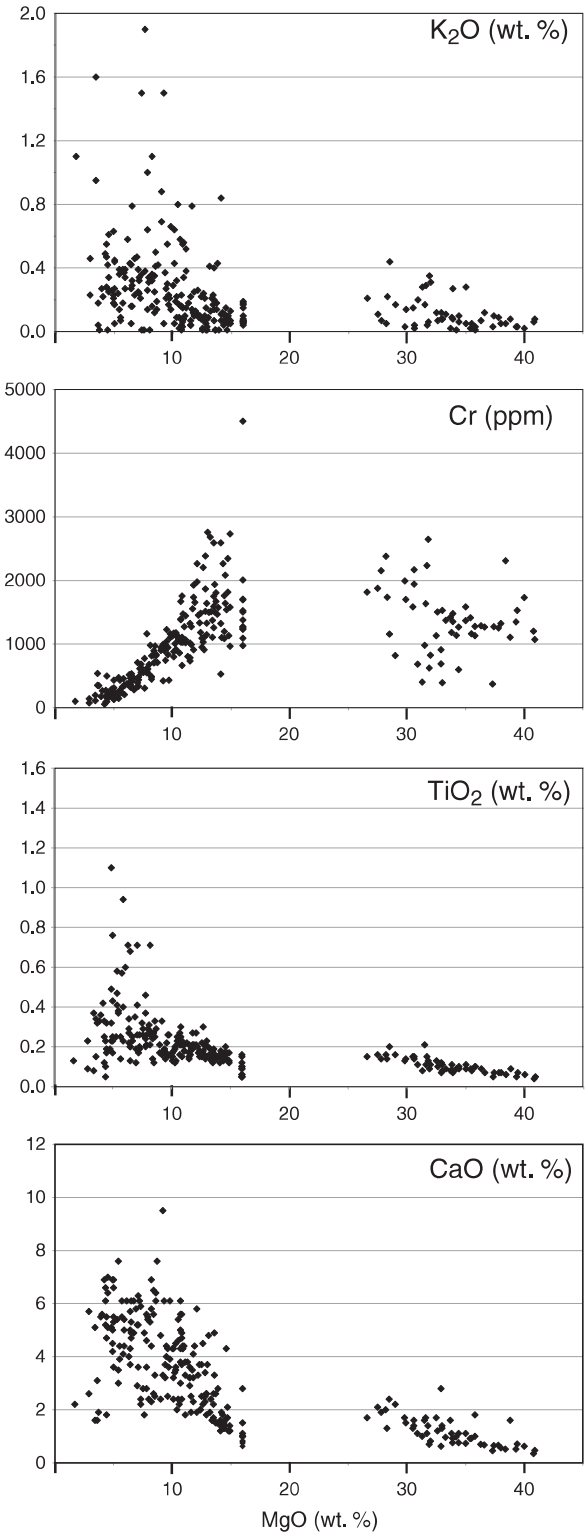

Fig. 5. Plot of MgO versus K_2O, Cr, TiO_2 and CaO for the whole length of drill core FSDM07.

The correlation of MgO content with CaO, TiO_2, K_2O and Cr for layered rocks of the drill hole FSTQ-01 (Fig. 9) is consistent with this sequence of crystallization of cumulus minerals.

Samples of peridotite (MgO>24 wt.%) and pyroxenite–gabbronorite (MgO<15 wt.%) form two distinct groups, as revealed by Fig. 8, and reveal the sharp contact between olivine-rich peridotite and pyroxenite, as well as the gradational transition between pyroxenite and gabbronorite. High MgO contents of peridotite samples (up to 35 wt.%; Figs. 8 and 9) are consistent with high MgO content of olivine (up to Fo_{90}) from peridotite reported by Silva (1997). Higher CaO and TiO_2 contents, when compared to data from the Damolândia Complex, are consistent with the abundance of clinopyroxene in the layered rocks, while high Cr contents are consistent with the presence of chromite in both peridotite and pyroxenite. Higher CaO contents are particularly significant in peridotites, indicating the abundance of lherzolite in the Taquaral Complex, while harzburgite predominates in the Damolândia Complex. Higher Ti contents in gabbronorite of the Taquaral Complex is associated with disseminated ilmenite. Scattered high contents of K_2O are associated with disseminated interstitial phlogopite. Similar to what was described for the Damolândia Complex, high K_2O contents show no correlation with MgO content suggesting that they result from inhomogeneous assimilation of crustal rocks by the parental magma.

Rocks with metamorphic mineralogy and tectonic texture prevail throughout the layered sequence of drill core FSTQ-01. In these zones the primary igneous mineralogy is recrystallized into fine-grained metamorphic minerals. Recrystallized mafic rocks consist of fine-grained granoblastic aggregates of plagioclase, orthopyroxene, clinopyroxene, dark-brown amphibole and minor spinel (Fig. 7H), indicating that recrystallization occurred under conditions of high temperature (granulite facies of regional metamorphism). Mafic rocks associated with silimanite–garnet leptynite in the upper part of the drill core are similar to highly tectonized gabbronorite of the layered sequence, which suggests that they represent disrupted fragments of the layered sequence.

An elongated body of coarse-grained porphyritic orthogneiss occurs in the northwestern corner of the area investigated by INV (Fig. 6). This orthogneiss has granitic composition and was sampled for isotopic studies (sample TAQ-03).

4.2. Samples and isotopic results

4.2.1. Damolândia region

Sample DM-16 is a leucogabbro corresponding to a residual, late-stage influx of magma that cut across other partially crystallized rocks. The analyzed drill core sample from the Damolândia Layered Complex (FSDM07, Fig. 2) corresponds to a heterogeneous interval in terms of metamorphism, in which strongly deformed and metamorphosed areas with polygonal mineral boundaries co-exist with relict igneous pyroxene grains (Fig. 3F).

Zircon crystals occur either within adcumulate phases or within plagioclase and hornblende crystals. They are commonly bordered by intergrowths of ilmenite and magnetite. Zircon crystals are pristine, colorless to pink and show stubby to prismatic habit with varied degree of rounding. Generally, grains are fragmented and their widths vary between 300 and 800 μm. Under cathodoluminescence, they show well defined sector zoning and are surrounded by a thin, bright outer rim with irregular boundaries (Fig. 10A). Zircon usually contains inclusions of apatite, pyrite and ilmenite, around which recrystallization also occurs.

Eighteen U–Pb spot analyses render a chain of concordant to nearly concordant ages spreading from 670 Ma down to 590 Ma (Fig. 11A; Table 1). There is no obvious correlation between internal structure of the crystal and U–Pb data, since there are grains with similar ages (within error) in both rim and core (Table 1). Lu–Hf analyses reveal $^{176}Hf/^{177}Hf_t$ ratios between 0.282119 and 0.282290, and strongly negative $\varepsilon_{Hf(T)}$ signature, ranging from −3.06 to −9.83 (Table 2). Two-stage hafnium model ages yield $T_{(DM)}$ values from 1.60 to 1.93 Ga.

Nd isotopic data obtained for the Damolândia Layered Complex render Nd model ages between 1.78 and 2.16 Ga, with strongly negative ε_{Nd} ($T=650$ Ma) values (−3.9 to −26.5) (Table 3). The Sm–Nd data, plotted against the stratigraphy of the drill hole FSDM-07, reveals that the ε_{Nd} values do not correlate with the layering sequence

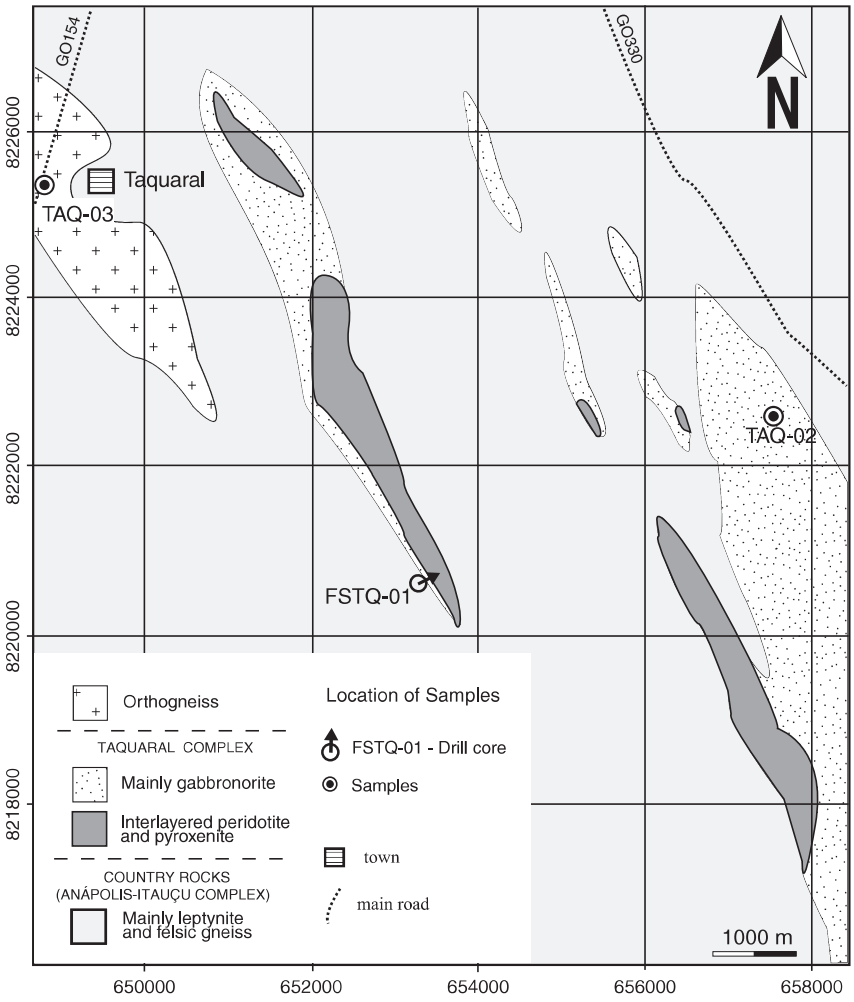

Fig. 6. Geology of the northern area of the Taquaral Complex (from unpublished report of International Nickel Venture Ltd.; UTM coordinate system, datum SAD-69, zone 22).

and, therefore the observed variation is related merely to different degrees of assimilation during the emplacement in an older continental crust (Fig. 4).

Sample DM-20 corresponds to a strongly foliated mafic granulite with dioritic composition, exposed near (~2.5 km) an occurrence of sapphirine + quartz bearing granulites (sample PT-62; Baldwin et al., 2005; Moraes et al., 2002). In sample DM 20, zircon is included in plagioclase crystals and also occurs close to hornblende corona. Zircon grains are approximately 150 μm long and are pristine and colorless. Commonly, these crystals show a "soccer-ball" habit, with rounded terminations, typical of zircon growth under granulite facies conditions (Schaltegger et al., 1999; Vavra et al., 1999). Primary internal texture in igneous crystals is represented by sector zoning, which is partially preserved in some grains, while featureless zircon is the main metamorphic texture. Some grains also show bright, luminescent rims with lobate, curved inward boundaries (Fig. 10B). Generally, these luminescent domains provide highly discordant U–Pb ages.

Ten spot analyses yield a spread of concordant ages from 670 to 530 Ma (Fig. 11B; Table 4) and identical ages are identified in rims and cores, similar to that previously described for sample DM-16. $^{176}Hf/^{177}Hf_t$ ratios range from 0.282291 to 0.282583 and $\varepsilon_{Hf(T)}$ vary in the interval of 5.73 to −3.65. Two-stage hafnium model ages reveal values from 1.05 to 1.60 Ga (Table 5).

Dioritic granulites, contrary to the mafic–ultramafic complex, show younger Nd model ages (1.2 Ga) and only slightly negative ε_{Nd} ($T = 650$ Ma) values (−0.72; Table 3). This might indicate either a different degree of assimilation of older continental crust or even that these rocks were generated from a distinct, more depleted magma source.

4.2.2. Taquaral area

TQ-14 is an amphibolite from the Taquaral Layered Complex drill core sample (FSTQ-01; Fig. 6). Zircon grains occur included in plagioclase and hornblende. They are pristine, colorless and

Fig. 7. A) Boulder of highly foliated mafic granulite of the Taquaral Complex. The mineral assemblage consists of orthopyroxene, clinopyroxene, plagioclase, hornblende and magnetite. Abundant reddish termite mounts are developed on soil from mafic rocks (sample TAQ-02). B) Outcrop of highly foliated subvertical peridotite. Elongated pyroxene crystals and pyroxene aggregates become evident in the weathered surface. C) Sharp contact between peridotite (left part) and pyroxenite (right part) from drill core FSTQ-01. Large pyroxene crystals in the peridotite show up in lighter colors. D) Photomicrograph of peridotite consisting of partially serpentinized olivine crystals (Ol) associated with large orthopyroxene (Opx) and chromite (Cr). E) Orthopyroxenite with interstitial sulfides from drill core FSTQ-01. F) Photomicrograph of orthopyroxenite consisting of cumulus orthopyroxene (Opx) and interstitial sulfides (Sulf) and plagioclase (white and low relief minerals) G) Photomicrograph of gabbronorite from FSTQ-01. Ilmenite (opaque) and phlogopite (small brownish lamellae) are accessory minerals. H) Photomicrograph of recrystallized mafic rock from drill hole FSTQ-01. This sample is a mafic granulite with fine-grained granoblastic texture. The mineral assemblage consists of orthopyroxene (Opx), clinopyroxene (Cpx), brownish hornblende (Hbl), plagioclase (Pl), ilmenite (opaques) and spinel (small greenish crystals associated with ilmenite).

commonly show stubby to prismatic habit, with sharp to rounded surfaces. The crystals vary in size from 200 μm to 500 μm. Bright, luminescent cores with weak sector zoning usually present very low Pb contents and reveal highly discordant and occasionally younger U–Pb ages than that observed in the correspondent rim. These cores are surrounded by a dark domain and some grains also have a very thin

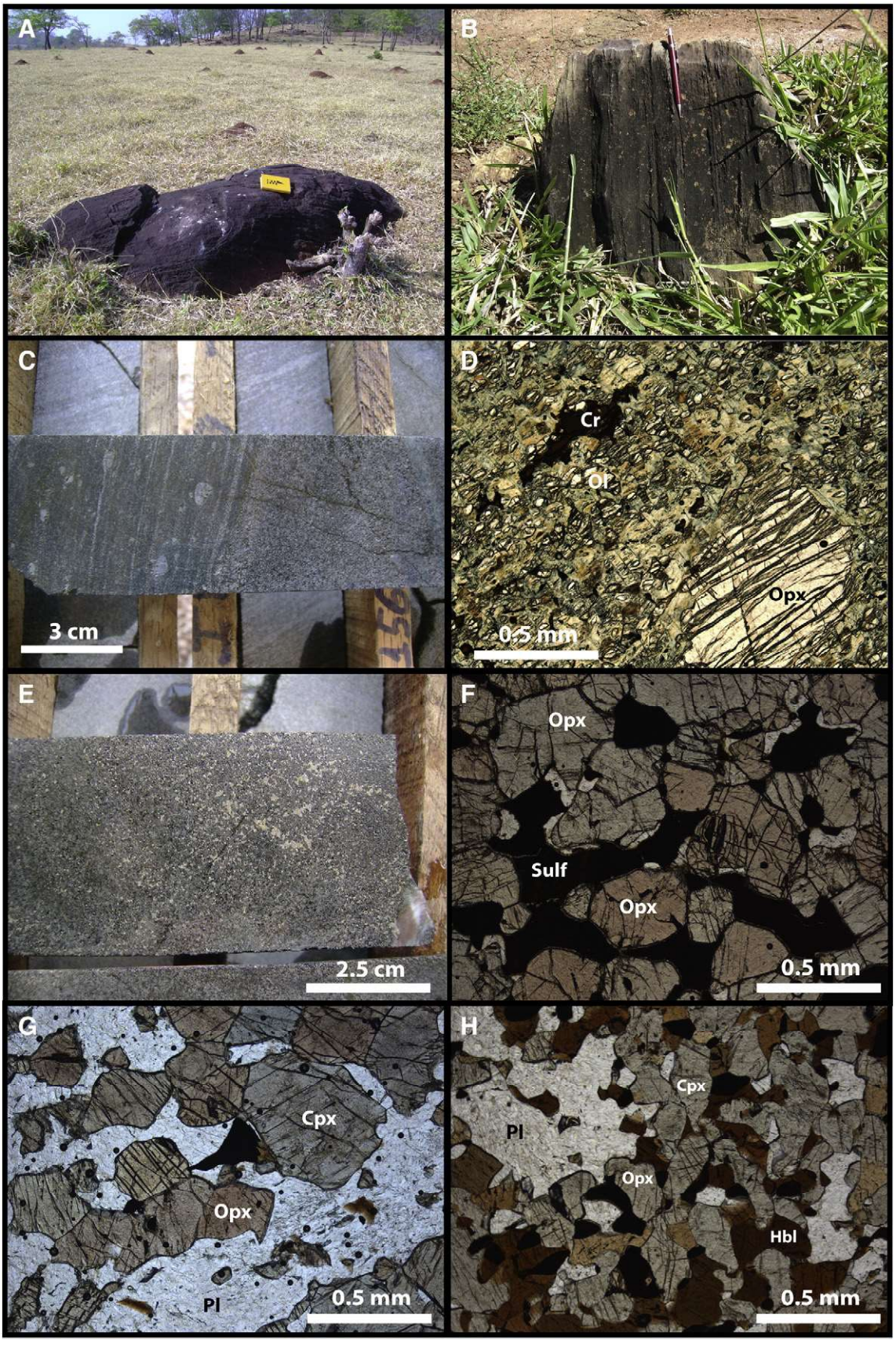

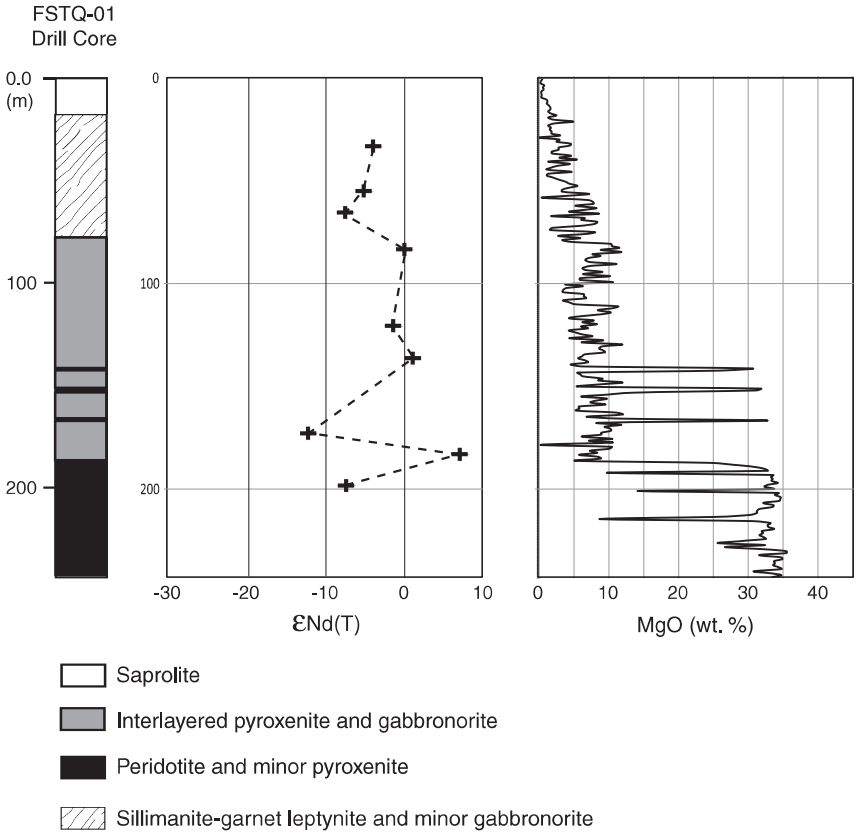

Fig. 8. Log, $\varepsilon_{Nd(T)}$ and MgO content for drill core FSTQ-01 in Taquaral Complex (see Fig. 6 for location).

and brilliant external rim (Fig. 10C). In addition, structureless zircon is recurrent.

Thirteen spot analyses reveal concordant ages varying from 670 to 585 Ma (Fig. 11C, Table 6). As observed in the Damolândia Complex, the scatter of ages cannot be linked to internal features in zircon grains. Hf isotopic ratios of these crystals range from 0.282197 to 0.282341, with strongly negative $\varepsilon_{Hf(T)}$ values (from −1.86 to −7.03). Two-stage Hf model ages vary between 1.51 and 1.69 Ga (Table 7).

Sample TAQ-02 corresponds to a medium-grained gabbronorite with granoblastic texture (see Fig. 6 for location). Zircon crystals are pristine and occur as stubby to prismatic grains, usually fragmented and smaller than 300 μm. BSE imaging reveals the existence of cores with relict sector zoning, which are surrounded by a bright, outer domain with curved, irregular boundaries (Fig. 10G). Featureless crystals are also commonly observed. Ten SHRIMP spot analyses yield variable discordant results, with $^{206}Pb/^{238}U$ ages ranging from 623 Ma to 525 Ma (Fig. 11D; Table 8).

In the Taquaral Complex, Nd model ages are slightly younger than that observed in the Damolândia Complex (1.36 to 1.92 Ga) and ε_{Nd} (T = 650 Ma) varies from +0.1 to −7.8 (Table 9). The deviation in the ε_{Nd} value reflects varied degrees of crustal contamination, similar to that described for the Damolândia Complex (Fig. 8).

Sample TAQ-03 corresponds to a porphyritic biotite orthogneiss exposed in the western margin of the mafic complex (Fig. 6). It consists of pink, clear elongated and prismatic (4:1) zircon grains. Inclusions or fractures are rare. Four zircon fractions were investigated by conventional ID-TIMS and yielded highly discordant U–Pb data. However, the upper intercept age of 631 ± 24 Ma (MSWD = 8.1, Fig. 11E, Table 9) is interpreted as being representative of the igneous crystallization.

4.2.3. Goianira–Trindade Complex

The Goianira–Trindade Complex is an additional mafic–ultramafic complex that occurs within the AIC, to the south of the Damolândia layered body (see Fig. 1B for location). It is composed of peridotite, pyroxenite and gabbronorite, with varied degrees of deformation and high-grade metamorphic overprint, similar to that described in the Damolândia and Taquaral complexes.

Sample INHO-01 is a coarse-grained leucogabbro in which two zircon populations can be distinguished (670357E/8172190N; datum SAD-69, zone 22). Small, prismatic grains characterize the first group, whereas the second is composed of colorless, rounded crystals with stubby habit, typical of metamorphic growth. However, there is no correlation among the data obtained and zircon population. ID-TIMS analyses of seven fractions reveal variably discordant results with a cluster of $^{206}Pb/^{238}U$ ages around 620 Ma, whereas one fraction yield a value of 662 Ma (Fig. 11F, Table 11).

Nd isotopic data obtained for seven cogenetic rocks from the Goianira–Trindade Complex reveal positive to slightly negative ε_{Nd} values (−0.93 to +3.18) and T_{DM} Nd model ages between 1.10 and 1.28 Ga (Table 12). The results suggest derivation from a depleted mantle, with restricted crustal contribution.

5. Discussion

5.1. "Metamorphic" zircon and the spread of U–Pb ages

Zircon is a common mineral in almost all rock types and occurs in a wide range of environments, ranging from the Earth's surface to deeper crustal levels. Owing to its resilience, even in such extreme conditions, zircon allows the link between *P–T* paths and geological

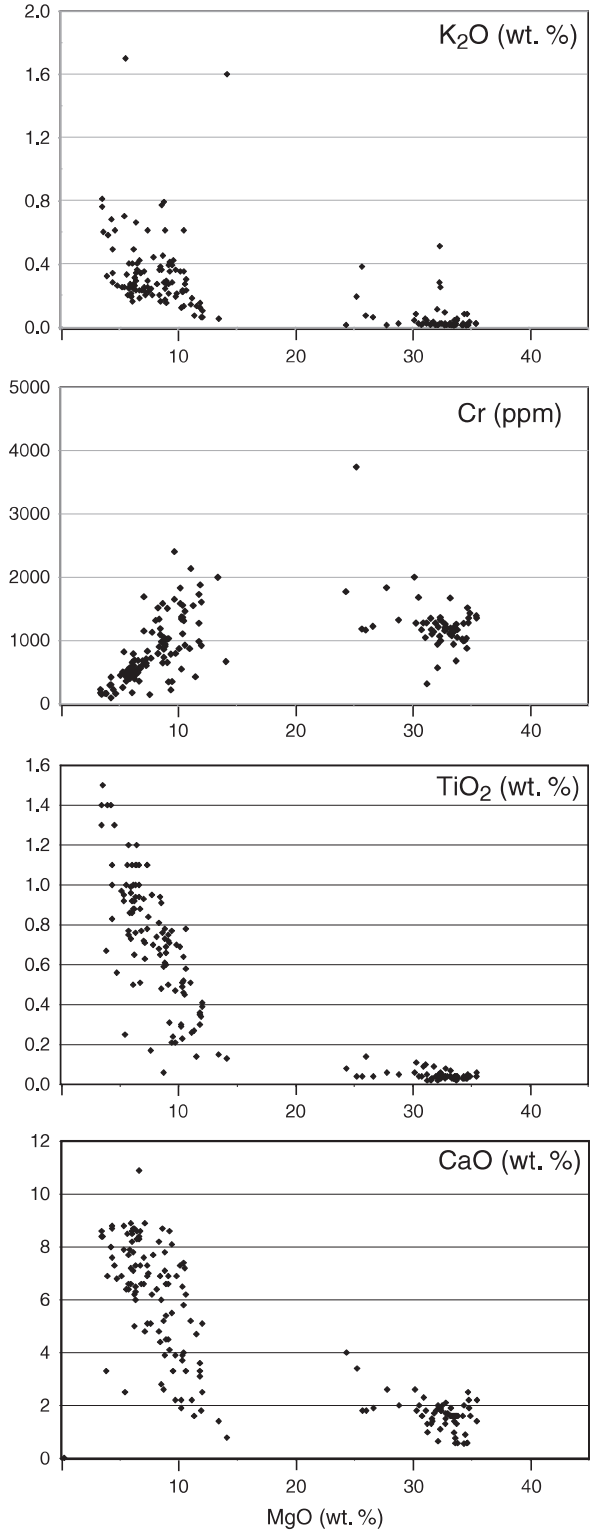

Fig. 9. Plot of MgO versus K_2O, Cr, TiO_2 and CaO for the whole length of drill core FSTQ-01.

time. However, recent studies have shown that processes taking place during high-grade metamorphism affect the U–Pb isotopic signature of zircon.

In granulite facies, zircon may display two distinct behaviors as a response to the extraordinary pressure and temperature conditions. *New zircon growth* may occur either in the subsolidus state, due to the breakdown of Zr-bearing minerals in metamorphic reactions, or from a melt/fluid phase (Ayers et al., 2003; Bingen et al., 2001; Degeling et al., 2001; Fraser et al., 1997; Möller et al., 2003; Roberts and Finger, 1997; Rubatto, 2002; Rubatto and Hermann, 2007; Schaltegger et al., 1999; Vavra et al., 1999; Whitehouse and Platt, 2003). Growth of new zircon results in the overgrowth of older grains or in the crystallization of a new population of individual crystals. In general, zircon generated under such conditions is pristine and small. Their external and internal patterns are variable, as they might form prisms with oscillatory zoning (Nystrom and Kriegsman, 2003), as well as equant, granoblastic crystals with "soccer-ball" habit (Schaltegger et al., 1999; Vavra et al., 1999). However, the new zircon commonly shows different geochemical signature compared to the protolith igneous grain, since it crystallizes in (i) a chemically distinct environment, or (ii) in equilibrium with other minerals, such as garnet and monazite, which can influence the partition coefficient of important constituents of zircon (Bingen et al., 2001; Rubatto, 2002; Rubatto and Hermann, 2007). Besides that, because of the complete opening of the isotopic system, their ages and isotope ratios are distinguishable from older crystals and, hence, newly grown zircon records younger geological events.

Conversely, zircon can *re-equilibrate* in the presence of a fluid or a melt phase (Ashwal et al., 1999; Corfu et al., 2003; Hoskin and Black, 2000; Martin et al., 2008; Schaltegger et al., 1999; Vavra et al., 1999). Under CL images, crystals that have experienced such alteration show an irregular and diffuse, curved inward boundary (Corfu et al., 2003; Geisler et al., 2007; Hoskin and Black, 2000). Occasionally, primary structures are partially preserved, rendering a "ghost" feature in the altered zone (Hoskin and Black, 2000).

In this scenario, if the crystal is radiation-damaged, the defects may enhance the diffusion of elements in zircon, promoting both the gain of common Pb and unusual cations (Ca, Al, and Fe) and the loss of essential components, such as Zr, Si, Pb, Hf, REE and U (Geisler et al., 2007; Schaltegger et al., 1999; Vavra et al., 1999). Consequently, the diffusion reaction process usually yields discordant U–Pb analyses.

However, if zircon is crystalline, re-equilibrium occurs dynamically in a coupled dissolution–reprecipitation process, in which the system remains closed (or partially closed) for the main components (Ashwal et al., 1999; Geisler et al., 2007; Martin et al., 2008; Putnis, 2002; Tomaschek et al., 2003). If the equilibrium is not complete, the crystal retains part of the isotopic and geochemical information of the original grain. Accordingly, such zones can provide intermediate ages between primary, crystallization ages, and secondary, metamorphic or hydrothermal alteration and, therefore, their geological meaning may not be real (Geisler et al., 2007; Hoskin and Black, 2000; Mezger and Krogstad, 1997; Möller et al., 2002).

Since the Lu–Hf isotopic system is decoupled from U–Pb systematics during zircon alteration, it has been used to unravel distinct geological events related to high-grade metamorphic overprint (Gerdes and Zeh, 2009; Sláma et al., 2007; Xia et al., 2009). In contrast to CL imaging and trace element analysis, Hf isotopes allow verifying different episodes of new zircon growth based on the fact that individuals formed within an isotopically homogeneous magmatic suite and/or in the same geological event shall yield similar initial Hf isotopic ratios (Gerdes and Zeh, 2009; Nebel et al., 2007).

As discussed in the previous section, there is a variation in the Hf isotopic signature of Damolândia and Taquaral zircon grains (Tables 2, 5 and 7). This behavior may be attributed to different degrees of interaction between mantle-derived melts and older crustal components, which is also corroborated by the Nd whole-rock data (Tables 3 and 10). However, neither the Hf isotopic ratios nor the $\varepsilon_{Hf(T)}$ can be linked to any specific zircon age domain. As shown in Fig. 12, the Hf data scatter randomly along the $^{206}Pb/^{238}U$ axis, revealing no correlation with the large spread of concordant U–Pb ages, which suggests that the oscillation of Hf isotopic signature is related merely to crustal contamination and, therefore, all zircon crystals (within individual samples) were grown in a single geological episode.

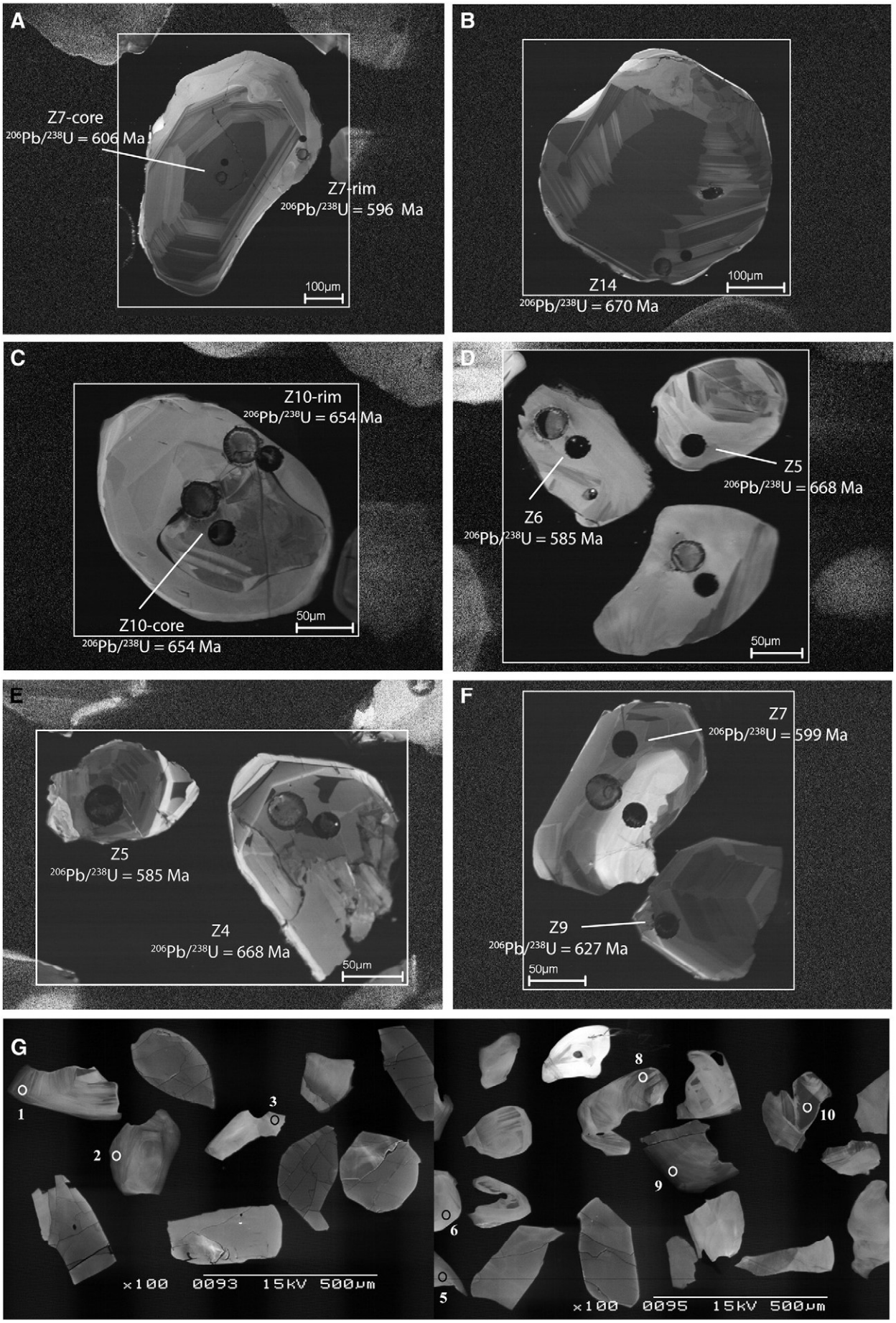
A
Z7-core
$^{206}Pb/^{238}U$ = 606 Ma
Z7-rim
$^{206}Pb/^{238}U$ = 596 Ma
100µm
B
Z14
$^{206}Pb/^{238}U$ = 670 Ma
100µm
C
Z10-rim
$^{206}Pb/^{238}U$ = 654 Ma
Z10-core
$^{206}Pb/^{238}U$ = 654 Ma
50µm
D
Z5
$^{206}Pb/^{238}U$ = 668 Ma
Z6
$^{206}Pb/^{238}U$ = 585 Ma
50µm
E
Z5
$^{206}Pb/^{238}U$ = 585 Ma
Z4
$^{206}Pb/^{238}U$ = 668 Ma
50µm
F
Z7
$^{206}Pb/^{238}U$ = 599 Ma
Z9
$^{206}Pb/^{238}U$ = 627 Ma
50µm
G
1
2
3
×100 0093 15kV 500µm
5
6
8
9
10
×100 0095 15kV 500µm

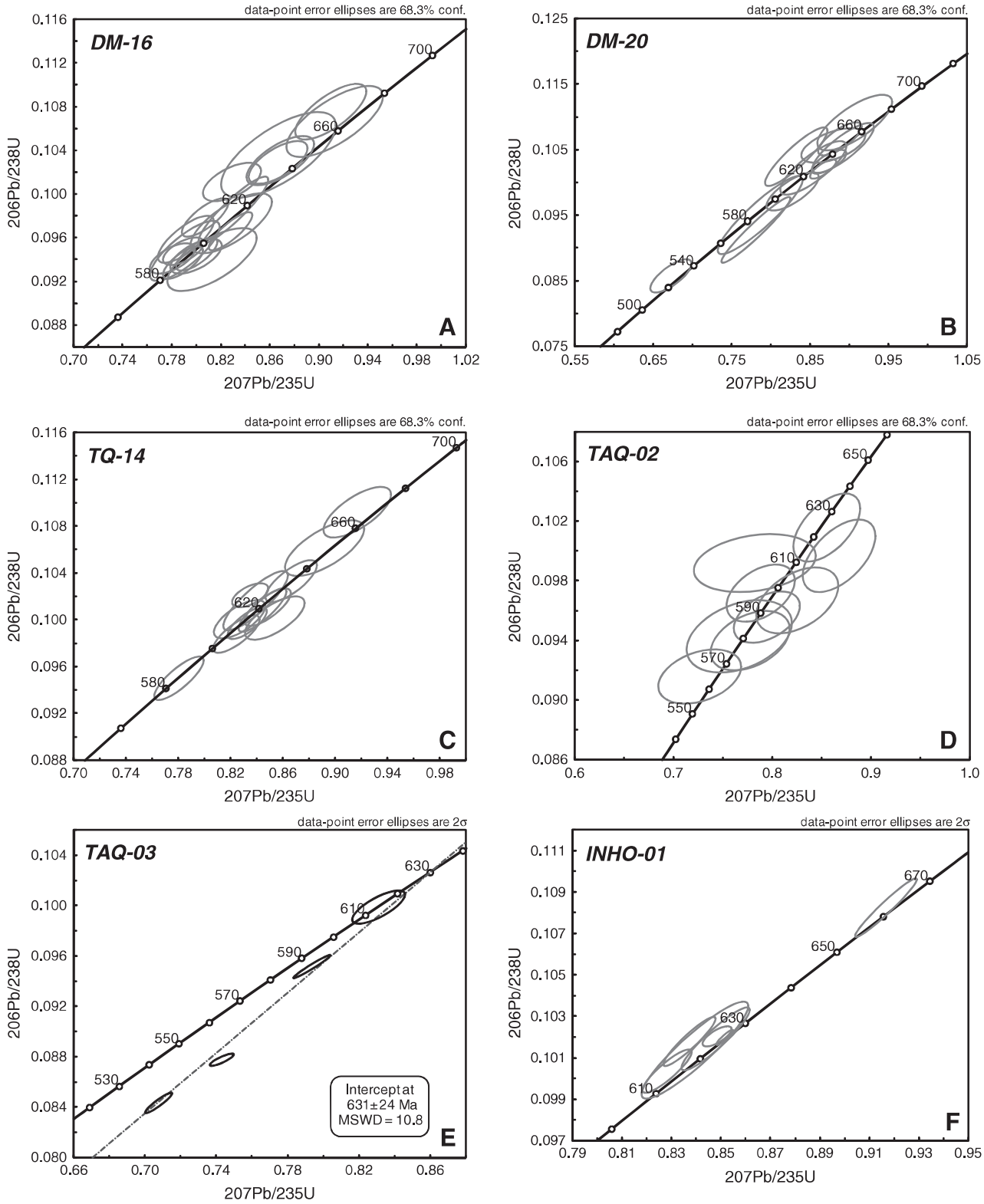

Fig. 11. LA-MC-ICPMS (A–C), SHRIMP (D) and ID-TIMS (E–F) U–Pb plots for Damolândia (DM), Taquaral (TQ, TAQ) and Goianira–Trindade complexes (INHO).

Since high-grade metamorphism does not disturb the Lu–Hf systematic in zircon grains, the Hf isotopic ratios should evidence the primary growth of zircon and, hence, the older ages, around 670 Ma, may be interpreted as representative of the emplacement of the Damolândia and Taquaral mafic–ultramafic complexes.

Furthermore, the Hf isotopic signature supports that, during metamorphism of these complexes, zircon *re-equilibrated* rather than *re-grew*. This is also justified by the CL characteristics of the crystals, in which curved, inward-moving boundaries are frequent. The fact that all individuals reveal concordant to nearly concordant

Fig. 10. CL images of zircon from sample DM-16 (A, B), sample DM-20 (C, D) and sample TQ-14 (E, F) and BSE image of sample TAQ-02 (G). Smaller spots on CL images (30 μm) represent the location of U–Pb analyses, whereas larger spots (40 μm) correspond to Hf isotopic investigation.

Table 1
U–Pb LA-MC-ICPMS data for sample DM-16.

Sample	*f* (206)%	Th/U	6/4 ratio	7/6 ratio	1s (%)	7/5 ratio	1s (%)	6/8 ratio	1s (%)	Apparent ages						Rho	Conc (%)
										7/6 age	2σ	7/5 age	2σ	6/8 age	2σ		
004-Z1	0.19	0.26	11848	0.05912	1.1	0.7891	1.4	0.09680	0.9	571.6	47	590.6	12.4	595.6	9.8	0.61	104
005-Z2	0.11	0.20	15807	0.06020	1.3	0.7996	1.7	0.09633	1.1	610.8	58	596.6	15.6	592.9	12.2	0.62	97
008-Z3	0.62	0.22	2884	0.05863	1.2	0.7915	1.9	0.09791	1.4	553.3	53.8	592.0	17	602.2	16.6	0.76	109
009-Z4	0.20	0.16	11349	0.05887	1.2	0.7803	1.5	0.09613	1.0	562.3	52.8	585.6	13.8	591.7	10.8	0.61	105
010-Z5	0.23	0.19	7649	0.06010	0.9	0.8000	1.4	0.09654	1.0	607.2	40.8	596.8	12.6	594.1	11.8	0.74	98
011-Z6	0.21	0.18	8499	0.06046	1.9	0.8283	2.7	0.09937	1.8	619.9	83.6	612.6	24.4	610.7	21.2	0.72	99
014-Z7-RIM	0.32	0.21	5512	0.05920	1.4	0.7904	2.4	0.09683	1.9	574.5	61.4	591.4	21.2	595.8	21.4	0.80	104
015-Z7-CORE	0.12	0.27	14087	0.06089	0.8	0.8278	1.4	0.09861	1.2	635.3	34.2	612.4	13.2	606.2	13.8	0.84	95
016-Z8	0.09	0.20	18741	0.05973	0.9	0.7888	1.4	0.09578	1.0	593.8	39.8	590.5	12.2	589.6	11.4	0.75	99
017-Z9	0.14	0.18	13115	0.06138	2.2	0.8127	3.0	0.09602	2.0	652.6	95.6	604.0	27	591.1	22.2	0.68	91
021-Z10	0.09	0.20	19111	0.05861	1.0	0.8070	1.5	0.09986	1.2	552.7	43.8	600.8	14	613.6	13.6	0.76	111
022-Z11	0.14	0.20	2190	0.05993	1.5	0.8683	2.1	0.10508	1.4	601.2	66.2	634.7	19.6	644.1	17.4	0.68	107
023-Z12	0.11	0.25	16144	0.05832	1.5	0.8291	1.9	0.10311	1.1	541.6	66.8	613.1	17.4	632.6	13.4	0.58	117
024-Z13	0.12	0.18	14238	0.05951	2.6	0.8667	3.6	0.10563	2.4	585.7	113.8	633.8	33.8	647.3	30	0.69	111
027-Z14	0.25	0.18	7118	0.06020	1.4	0.9093	2.1	0.10955	1.5	610.8	62.6	656.7	20.4	670.1	19.6	0.73	110
028-Z15	0.18	0.20	8927	0.05989	1.4	0.8665	1.8	0.10494	1.2	599.5	58.6	633.7	17.2	643.3	15	0.67	107
029-Z16	0.27	0.29	6526	0.05986	1.0	0.8300	2.2	0.10056	2.0	598.5	42	613.6	20.8	617.7	24	0.91	103
030-Z17	0.20	0.32	8744	0.06093	2.1	0.9129	2.9	0.10866	2.0	636.9	88.6	658.6	27.6	665.0	25	0.71	104

Table 2
Summary of in situ Lu–Hf analyses for sample DM-16.

Sample	$^{176}Lu/^{177}Hf$	2σ	$^{176}Hf/^{177}Hf$	2σ	Age (Ma)	$(^{176}Hf/^{177}Hf)_t$	2σ	$\varepsilon_{Hf(T)}$	1σ	$T_{(DM)}$ (Ga)
003-Z1	0.0004016	±0.000005	0.282129	0.000025	596	0.282124	0.000025	−9.83	±0.40	1.93
004-Z2	0.0004241	±0.000000	0.282198	0.000030	593	0.282193	0.000030	−7.47	±0.55	1.80
005-Z7-RIM	0.0003607	±0.000002	0.282236	0.000025	596	0.282232	0.000025	−6.03	±0.39	1.73
006-Z7-CORE	0.0006237	±0.000003	0.282159	0.000029	606	0.282152	0.000029	−8.63	±0.51	1.88
009-Z6	0.0002894	±0.000002	0.282229	0.000026	611	0.282226	0.000026	−5.92	±0.40	1.73
010-Z11	0.0003603	±0.000001	0.282290	0.000038	644	0.282285	0.000038	−3.07	±0.82	1.60
011-Z12	0.0004843	±0.000001	0.282193	0.000028	633	0.282187	0.000028	−6.79	±0.47	1.80
012-Z13	0.0003522	±0.000000	0.282156	0.000034	647	0.282151	0.000034	−7.74	±0.67	1.86
015-Z15	0.0003595	±0.000000	0.282123	0.000038	643	0.282119	0.000038	−8.98	±0.80	1.92
016-Z14	0.0004665	±0.000004	0.282195	0.000036	670	0.282189	0.000036	−5.91	±0.72	1.78
017-Z4	0.0005511	±0.000003	0.282231	0.000023	592	0.282225	0.000023	−6.36	±0.34	1.74
018-Z5	0.0003581	±0.000002	0.282220	0.000025	594	0.282216	0.000025	−6.64	±0.39	1.76

ages and that there is no evidence of a radiation-damage effect in the analyzed grains suggests that crystals might have experienced a concomitant dissolution–reprecipitation process. In view of this, the observed spread of ages in the Concordia diagram probably corresponds to intermediate values between igneous crystallization and the final closure of the U–Pb isotopic system, following the high-grade metamorphism.

Nonetheless, it is still not possible to distinguish a clear peak metamorphic age for the studied rocks based only on zircon analyses. Further research on rutile and other metamorphic minerals and might help to elucidate this question in the future.

The geochronological framework described here is similar to that of the Napier Complex, Antarctica (Kelly and Harley, 2005) and, likewise, suggests that the studied rocks were kept in high temperatures for a long time. This unusually hot condition might be achieved in deep levels in the crust, where igneous crystallization and metamorphic overprint are concomitant. Moreover, it may promote the partial opening of the U–Pb system in zircon and, consequently, produce the large spread of ages observed in the AIC.

5.2. Resolution of dating techniques

Another essential aspect when interpreting U–Pb data is the method used for dating. ID-TIMS ages are obtained from the dissolution of a randomly, optically selected grain and, occasionally, from more than one

Table 3
Sm–Nd data for the Damolândia Complex.

Sample	Lithotype	Prof. (m)	Sm (ppm)	Nd (ppm)	$^{147}Sm/^{144}Nd$	$^{143}Nd/^{144}Nd$	$(^{143}Nd/^{144}Nd)i$	$\varepsilon_{(0)}$	$\varepsilon_{(T)}$	T_{CHUR} (Ma)	T_{DM} (Ma)
DM 01	Gabbro	283.0	2.3296	9.4894	0.1484	0.512159	0.511527	−9.34	−5.34	1503	2046
DM 02	Gabbro	282.4	2.5896	11.0190	0.1421	0.512162	0.511557	−9.29	−4.75	1321	1857
DM 03	Norite	280.9	1.7779	7.8426	0.1370	0.511029	0.510445	−31.39	−26.48	–	–
DM 04	Norite	276.4	1.7122	7.2050	0.1437	0.512083	0.511471	−10.82	−6.43	1585	2073
DM 05	Norite	241.5	1.8431	6.5716	0.1695	0.512323	0.511601	−6.14	−3.89	–	–
DM 07	Orthopyroxenite	217.8	0.6952	2.4391	0.1723	0.512198	0.511464	−8.58	−6.56	–	–
DM 08	Orthopyroxenite	216.0	0.8166	2.8761	0.1716	0.512303	0.511572	−6.53	−4.45	–	–
DM 10	Pyroxenite	209.4	4.1570	15.6256	0.1608	0.512360	0.511675	−5.42	−2.44	1171	1947
DM 14	Ol-Orthopyroxenite	102.2	0.4490	1.7858	0.1520	0.512162	0.511514	−9.29	−5.59	1614	2162
DM 15	Orthopyroxenite	99.3	0.7883	2.5250	0.1887	0.512024	0.511220	−11.98	−11.33	–	–
DM-16	Gabbronorite	68.0	4.6482	27.7413	0.1013	0.511722	0.511290	−17.88	−9.96	1458	1778
DM 18	Mafic granulite		18.7812	105.0402	0.1081	0.512223	0.511763	−8.09	−0.72	710	1176
DM 20	Mafic granulite		3.8743	12.3038	0.1903	0.512642	0.511831	0.09	0.61	–	–

Table 4
U–Pb LA-MC-ICPMS data for sample DM-20.

Sample	*f* (206)%	Th/U	6/4 ratio	7/6 ratio	1s (%)	7/5 ratio	1s (%)	6/8 ratio	1s (%)	Apparent ages						Rho	Conc (%)
										7/6 age	2σ	7/5 age	2σ	6/8 age	2σ		
005-Z2	0.65	0.13	2747	0.05679	1.7	0.6721	2.6	0.08583	2.0	483.4	77	522.0	21.4	530.8	19.8	0.75	110
013-z5	0.48	−0.02	3677	0.06019	2.3	0.9064	3.5	0.10923	2.6	610.3	99.8	655.1	33.4	668.2	32.6	0.75	110
014-z6	0.37	0.24	4609	0.05997	1.9	0.7862	4.5	0.09508	4.1	602.6	83.2	589.0	40.6	585.5	46	0.91	97
016-z8	0.23	0.25	7620	0.06054	1.9	0.8538	3.3	0.10229	2.6	623.0	82.6	626.8	30.6	627.8	31.6	0.82	101
021-z10-rim	0.34	0.14	5251	0.06141	1.6	0.8916	2.9	0.10530	2.4	653.7	69.4	647.2	27.8	645.4	29.6	0.83	99
022-z10-core	0.24	0.04	8689	0.06034	1.4	0.8875	2.1	0.10668	1.6	615.7	59.4	645.1	20	653.5	19.6	0.75	106
023-z11	0.33	0.19	5444	0.06138	2.0	0.8736	1.7	0.10322	1.2	652.7	85.8	637.5	15.6	633.2	14.2	0.72	97
028-z14	0.32	0.00	5792	0.06078	3.3	0.8270	2.7	0.09868	2.0	631.5	139.4	611.9	24.2	606.7	22.8	0.75	96
029-z15	0.12	0.03	14547	0.06154	0.8	0.8663	1.3	0.10209	1.0	658.3	35.6	633.6	12	626.7	11.6	0.77	95
030-z16	0.14	0.00	12996	0.06034	2.5	0.8792	3.0	0.10567	1.6	616.0	109.8	640.6	28.8	647.6	20.4	0.56	105
025-z19	0.30	0.16	5757	0.05805	1.5	0.8322	3.2	0.10397	2.8	531.7	63.8	614.8	29.2	637.6	34.2	0.89	120

Table 5
Summary of in situ Lu–Hf analyses for sample DM-20.

Sample	$^{176}Lu/^{177}Hf$	2σ	$^{176}Hf/^{177}Hf$	2σ	Age (Ma)	$(^{176}Hf/^{177}Hf)_t$	2σ	$e_{Hf(T)}$	1σ	$T_{(DM)}$ (Ga)
003-Z6	0.0003607	±0.000001	0.282587	0.000029	586	0.282583	0.000029	6.19	±0.53	1.04
005-Z8	0.0005757	±0.000001	0.282421	0.000046	628	0.282414	0.000046	1.14	±1.09	1.35
006-Z20	0.0001376	±0.000001	0.282375	0.000051	580	0.282373	0.000051	−1.36	±1.31	1.46
009-Z10-CORE	0.0000417	±0.000002	0.282447	0.000031	645	0.282447	0.000031	2.69	±0.57	1.28
010-Z10-RIM	0.0001762	±0.000004	0.282511	0.000042	654	0.282508	0.000042	5.04	±0.95	1.16
011-Z14	0.0000732	±0.000001	0.282292	0.000060	606	0.282291	0.000060	−3.70	±1.64	1.61
012-Z15	0.0001804	±0.000001	0.282519	0.000063	627	0.282517	0.000063	4.74	±1.71	1.15

Table 6
U–Pb LA-MC-ICPMS data for sample TQ-14.

Sample	*f* (206)%	Th/U	6/4 ratio	7/6 ratio	1s (%)	7/5 ratio	1s (%)	6/8 ratio	1s (%)	Apparent ages						Rho	Conc (%)
										7/6 age	2σ	7/5 age	2σ	6/8 age	2σ		
005-Z2	0.14	0.02	12260	0.05993	1.1	0.8269	1.6	0.10007	1.1	600.9	49.8	611.9	14.4	614.8	12.6	0.68	102
007-Z4	0.17	0.00	10215	0.06088	1.3	0.9169	1.9	0.10922	1.3	635.1	56.8	660.7	18	668.2	16.6	0.70	105
010-Z5	0.11	0.05	15679	0.05954	0.9	0.7801	1.6	0.09502	1.3	587.0	40.6	585.5	14.2	585.2	14.6	0.82	100
012-Z7	0.19	0.01	9530	0.05859	1.0	0.7865	1.4	0.09737	0.9	551.8	44.4	589.2	12	599.0	10.2	0.65	109
016-Z9	0.10	0.07	17716	0.05928	0.9	0.8346	1.1	0.10212	0.7	577.2	37.8	616.2	10	626.8	7.8	0.58	109
018-Z11	0.13	0.03	14002	0.06053	0.8	0.8324	1.2	0.09973	0.9	622.7	34.4	614.9	11	612.8	10.4	0.75	98
022-Z13	0.12	0.03	15039	0.06085	0.9	0.8482	1.4	0.10110	1.0	633.9	39.2	623.7	12.8	620.9	12.4	0.76	98
023-Z14	0.11	0.00	21400	0.06051	0.9	0.8243	1.4	0.09880	1.1	621.8	38.8	610.4	13	607.4	12.6	0.78	98
024-Z15	0.08	0.03	23582	0.06070	0.8	0.8442	1.5	0.10087	1.2	628.6	34.2	621.5	13.4	619.5	14.4	0.85	99
025-Z16	0.08	0.07	22193	0.06092	1.7	0.8917	2.2	0.10616	1.5	636.4	71.2	647.3	21.2	650.4	18.4	0.68	102
028-Z17	0.12	0.00	14569	0.05986	1.0	0.8390	1.9	0.10165	1.6	598.5	45	618.6	18	624.1	19.6	0.85	104
029-Z18	0.13	0.04	13054	0.06080	1.0	0.8661	1.5	0.10332	1.1	632.1	42.6	633.4	14.2	633.8	13.8	0.76	100
030-Z19	0.25	0.00	7064	0.06181	1.3	0.8536	1.7	0.10016	1.2	667.4	53.8	626.6	16.4	615.4	14.2	0.69	92

Table 7
Summary of in situ Lu–Hf analyses for sample TQ-14.

Sample	$^{176}Lu/^{177}Hf$	2σ	$^{176}Hf/^{177}Hf$	2σ	Age	$(^{176}Hf/^{177}Hf)_t$	2σ	$e_{Hf(t)}$	1σ	$T_{(DM)}$ Ga
004-Z2	0.0001583	±0.000003	0.282301	0.000065	615	0.282299	0.000065	−3.19	±1.80	1.59
005-Z4	0.0000923	±0.000001	0.282287	0.000040	668	0.282286	0.000040	−2.47	±0.85	1.59
006-Z5	0.0002344	±0.000004	0.282343	0.000064	585	0.282341	0.000064	−2.34	±1.78	1.52
009-Z7	0.0002078	±0.000001	0.282200	0.000073	599	0.282197	0.000073	−7.03	±2.08	1.79
011-Z11	0.0002111	±0.000012	0.282267	0.000057	612	0.282265	0.000057	−4.51	±1.50	1.65
012-Z14	0.0002436	±0.000005	0.282249	0.000039	607	0.282247	0.000039	−5.25	±0.87	1.69
013-Z15	0.0002784	±0.000006	0.282338	0.000049	619	0.282335	0.000049	−1.86	±1.21	1.51
014-Z16	0.0001586	±0.000002	0.282255	0.000048	650	0.282252	0.000048	−4.09	±1.15	1.66

Table 8
U–Pb SHRIMP data for sample TAQ-02.

Grain spot	% ^{206}Pb	U ppm	Th ppm	^{232}Th/^{238}U	ppm ^{206}Pb*	6/8 age	7/6 age	Conc (%)	207/206 ratio	±%	207/235 ratio	±%	206/238 ratio	±%	err corr
1.1	0.00	96	55	0.59	7.03	525.0 ± 6.3	633 ± 39	17	0.0608	1.8	0.712	2.2	0.0848	1.3	0.57
2.1	0.50	65	30	0.48	5.15	565.3 ± 7.3	510 ± 77	−11	0.0575	3.5	0.726	3.8	0.0916	1.3	0.36
3.1	0.42	32	16	0.52	2.60	581.1 ± 9.4	564 ± 94	−3	0.0589	4.3	0.766	4.6	0.0943	1.7	0.76
4.1	0.00	38	17	0.47	3.26	612.9 ± 9.1	709 ± 51	14	0.0630	2.4	0.867	2.8	0.0997	1.6	0.55
5.1	0.56	62	27	0.45	5.31	609.8 ± 7.7	498 ± 110	−22	0.0572	5.1	0.782	5.2	0.0992	1.3	0.25
6.1	0.00	47	30	0.65	4.07	623.6 ± 8.7	640 ± 47	3	0.0610	2.2	0.855	2.6	0.1016	1.5	0.56
7.1	0.32	55	25	0.47	4.47	579.4 ± 7.5	600 ± 68	3	0.0599	3.1	0.777	3.4	0.0940	1.4	0.40
8.1	0.27	46	22	0.51	3.81	594.8 ± 8.4	671 ± 64	11	0.0619	3.0	0.925	3.3	0.0967	1.5	0.44
9.1	0.25	68	36	0.55	5.72	598.1 ± 7.3	559 ± 56	−7	0.0588	2.6	0.788	2.9	0.0972	1.3	0.44
10.1	0.27	71	59	0.87	5.81	588.4 ± 7.0	612 ± 55	4	0.0602	2.5	0.794	2.8	0.0956	1.2	0.44

Table 9
U–Pb ID-TIMS data for sample TAQ-03.

Sample	# grains	Size (mg)	U ppm	Th ppm	Pb ppm	U/Th	206/204	Radiogenic ratios							Age			Ma
								207*/235	%	206*/238	%	rho	207*/206*	%	206*/238	207*/235	207*/206*	
TAQ03R	1	0.019	416.29	57.27	38.216	7.27	635	0.7073	0.89	0.0844	0.78	0.932	0.0608	0.23	522	543	632	9
TAQ03S	1	0.02	186.31	54.41	36.839	3.42	76	0.8305	1.45	0.0999	1.09	0.757	0.0609	0.8	608	614	636	36
TAQ03T	2	0.034	303.7	32.01	30.012	9.49	668	0.7428	0.74	0.0878	0.43	0.854	0.0614	0.21	542	564	653	11
TAQ03U	3	0.025	199.65	43.53	20.996	4.59	555	0.7932	1.09	0.0952	0.8	0.976	0.0604	0.21	586	593	620	7

crystal. As stated in the previous section, zircon that undergoes re-equilibration during metamorphism might preserve a component of the original isotopic information. Therefore, the main issue remains on whether ID-TIMS ages of zircon crystals from metamorphic terranes have a geological meaning or are only a geochronological artifact enhanced by a memory effect. Moreover, since only a few hand-picked zircon crystals are analyzed per sample, obtaining the correct crystallization age might also depend on "luck" when selecting the grains.

Such peculiarities may be shown in the sample INHO-01, in which U–Pb ID-TIMS analyses revealed a cluster of concordant to nearly concordant ages around 620 Ma, whereas only one fraction yielded a ^{206}Pb/^{238}U of 662 Ma (Table 11). The younger group of ages is analogous to other mafic–ultramafic complexes identified to the west of the AIC, in the domain of the Goiás Magmatic Arc (Laux et al., 2004). Additionally, titanite grains of a wollastonite–scapolite marble that occurs nearby the Goianira–Trindade Complex rendered an age of 632 Ma (Moraes et al., 2007).

Conversely, considering that re-equilibration of zircon grains during high-grade metamorphism was significant in some of the mafic–ultramafic intrusions within the AIC and that the older value obtained in sample INHO-01 is similar to that interpreted as the crystallization age for both Damolândia and Taquaral rocks, it suggests an analogous geochronological framework for the three layered complexes.

However, it is not possible to confirm neither of the interpretations above based only on the available U–Pb ID-TIMS data and, therefore, this method has shown to be inadequate for dating high-grade metamorphic terranes such as the AIC.

In-situ dating methods such as SIMS and LA-MC-ICPMS, for instance, have proven to be the more efficient technique in determining distinct geological events within one single grain, since it allows the analysis of all zircon domains, altered or not during metamorphism. Yet, the control of internal textures with CL or BSE imaging is a crucial condition for an accurate analysis and a correct interpretation of the ages obtained with these methods.

5.3. Tectonic implications for the evolution of the Brasília Belt

U–Pb zircon analyses of both Damolândia and Taquaral complexes revealed crystallization ages of ~670 Ma. Such values have already been reported in a previous study performed on the felsic high-grade rocks of the AIC (Piuzana et al., 2003a). However, older values were discarded as inheritance and concordia ages of ca. 645 Ma were accepted as representative of the timing of high-grade metamorphism in the AIC (Piuzana et al., 2003a).

Nevertheless, Möller et al. (2006) also reported 680 Ma zircon cores in UHT paragranulites, which were interpreted as zircon growth during a prograde path, in equilibrium with garnet. In addition, similar ages were obtained in rutile grains shielded in garnet, with Zr contents corresponding to peak temperatures (Möller et al., 2006; Zack et al., 2006). Therefore, the prograde metamorphic path of the

Table 10
Sm–Nd data for the Taquaral Complex.

Sample	Lithotype	Prof. (m)	Sm (ppm)	Nd (ppm)	^{147}Sm/^{144}Nd	^{143}Nd/^{144}Nd	(^{143}Nd/^{144}Nd)i	$\varepsilon_{(0)}$	$\varepsilon_{(T)}$	T_{CHUR} (Ma)	T_{DM} (Ma)
TQ 03	Gabbronorite	33.4	2.144	7.858	0.1649	0.512306	0.511603	−6.48	−3.85	1581	2293
TQ 05	Gabbronorite	55.2	7.981	29.540	0.1633	0.512238	0.511542	−7.81	−5.05	1814	2432
TQ 06	Orthopyroxenite	65.7	1.324	3.050	0.2624	0.512538	0.511420	−1.95	−7.42	–	–
TQ 08	Orthopyroxenite	83.6	2.121	8.847	0.1449	0.512424	0.511806	−4.18	0.12	626	1358
TQ 10	Gabbronorite	120.7	3.646	13.196	0.1670	0.512445	0.511733	−3.77	−1.31	982	1930
TQ 12	Gabbronorite	136.5	4.155	13.688	0.1835	0.512643	0.511862	0.11	1.21	–	–
TQ 15	Orthopyroxenite	173.0	0.638	1.200	0.3212	0.512547	0.511179	−1.78	−12.14	–	–
TQ 16	Gabbronorite	183.2	3.136	7.586	0.2499	0.513232	0.512168	11.59	7.18	–	–
TQ 18	Peridotite	198.4	0.099	0.189	0.3162	0.512773	0.511426	2.64	−7.31	–	–
TQ 22	Mafic granulite		5.893	22.327	0.1596	0.512354	0.511674	−5.54	−2.46	1157	1919

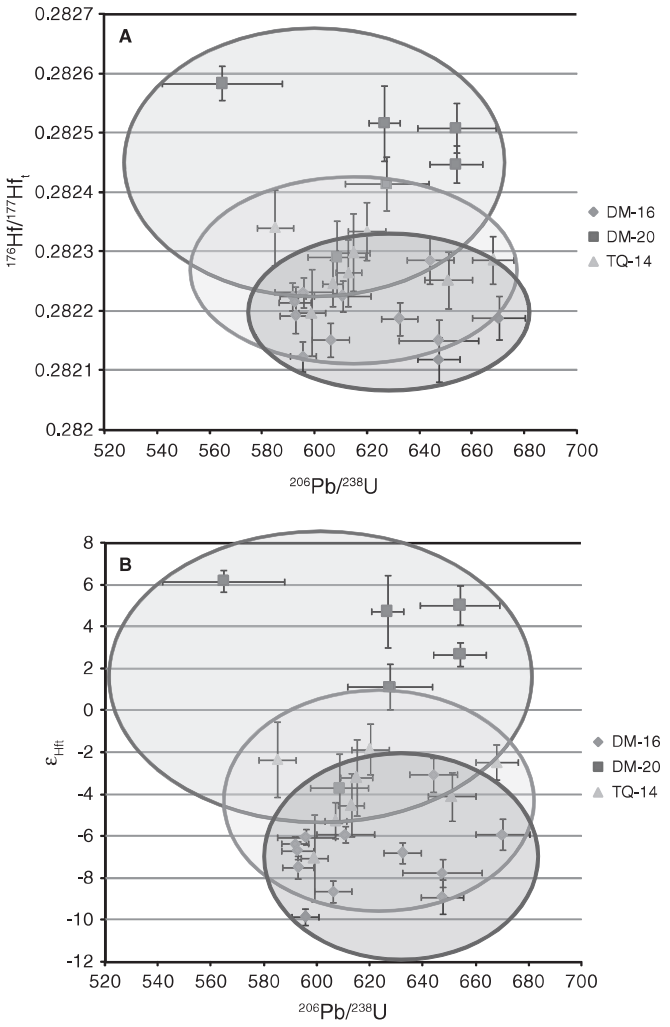

Fig. 12. Zircon in situ Hf isotopic data (A, $^{176}Hf/^{177}Hf_t$; B, ε_{Hft}) versus $^{206}Pb/^{238}U$ age plots.

paragranulites suggests that the prograde-to-peak UHT stage in the AIC may have occurred around 680–670 Ma, earlier than previously suggested. If so, at least part of the widespread mafic magmatism is coeval with the ultrahigh temperature metamorphic episode (Table 13).

However, 680–670 Ma ages are scarce in the Brasília Belt and are restricted to a few occurrences in the Goiás Magmatic Arc, to the west of the AIC (Laux et al., 2005; Pimentel et al., 2003a). Nevertheless, a recent geochronological investigation on retrograded eclogites in the southern sector of the Brasília Belt yielded an age of ca. 678 Ma, interpreted as representative of the close-to-peak metamorphism (Reno et al., 2009). Thus, these data reveal that, at 680–670 Ma, westward subduction and associated high-grade metamorphism were already occurring in the Southern Brasília Belt (Table 13).

Conversely, 650–640 Ma ages are widespread in the AIC. This stage is characterized by new zircon growth in felsic ortho- and paragranulites (Baldwin and Brown, 2008; Piuzana et al., 2003a) and might represent a post-peak metamorphic growth, probably due to the breakdown of Zr-bearing mineral phases and/or partial melting. In addition, structural data suggests that the D_1 greenschist to amphibolite facies metamorphism of the Araxá Group and the eastward emplacement of D_2 nappes in the southern Brasília Belt are associated with this period (D'el-Rey Silva et al., 2004; Table 13).

The post-peak decompressional melting and cooling stage of the AIC is marked by the growth of euhedral individual zircon crystals in opx-bearing leucossome at ca. 630 Ma, as well as by the crystallization of titanite grains in wollastonite–scapolite marble (Möller et al., 2006; Moraes et al., 2007; Table 13). Coeval to this period are a number of mafic–ultramafic intrusions in the domain of the Goiás Magmatic Arc, with crystallization ages of ~630 Ma (Laux et al., 2004), as well as coeval voluminous peraluminous granites in the AIC (Piuzana et al., 2003a; Table 13).

The emplacement of K-rich granites at 620 Ma along the Pireneus Syntaxis, a large-scale concave structure related to a WNW–ESE shortening (D_3 phase; D'el-Rey Silva et al., 2004, 2008; Fig. 1A), suggests a syn-tectonic origin for this magmatism (Pimentel et al., 2003b). This lithostructural deflection marks the final compressional stage caused by the collision between the Paranapanema and São Francisco cratons and, moreover, it is responsible for granulite exhumation in both southern and northern Brasília Belt (D'el-Rey Silva et al., 2004, 2008; Table 13).

Hence, in the collisional history of the orogen, there have been two distinct episodes of mafic magmatism: the older, around 670 Ma, related to the development of the UHT assemblages; and the latter, near 630 Ma, associated with decompressional melting and cooling after the metamorphic peak.

The geological framework described in this work, with voluminous mafic and felsic magmatism spatially and temporally associated with high-grade metamorphism, might correspond to extensional episodes within the collisional setting causing moderate thinning, during which the upwelling of the hot asthenosphere results in partial melting of both the mantle and continental crust, generating extensive mafic and felsic magmatism associated in space and time with ultrahigh temperature metamorphism.

6. Conclusions

Combined geological and new geochronological data on mafic–ultramafic rocks within the Anápolis–Itauçu Complex allow the following conclusions:

- The Damolândia and Taquaral intrusions correspond to layered mafic–ultramafic complexes, which partially preserve igneous

Table 11
U–Pb ID-TIMS data for sample INHO-01.

Sample	# grains	Size (mg)	U ppm	Th ppm	Pb ppm	U/Th	206/204	207*/235	Radiogenic ratios						Age			Ma
									%	206*/238	%	rho	207*/206*	%	206*/238	207*/235	207*/206*	
INHO7	3	0.022	566.71	57.345	49.46	0.09	3573	0.8484	0.56	0.1020	0.383	0.73	0.0603	0.386	626	624	614	8.3
INHO10	1	0.012	993.29	102.08	90.68	0.09	3536	0.8513	0.32	0.1020	0.296	0.91	0.0605	0.132	626	625	623	2.8
INHO8	5	0.017	94.138	11.537	64.01	0.68	483	0.9168	1.11	0.1083	1.07	0.96	0.0614	0.289	663	661	654	6.2
INHO2	4	0.026	140.52	15.063	41.85	0.30	928	0.8477	1.33	0.1019	1.22	0.92	0.0603	0.516	625	623	616	11
INHO5	4	0.026	147.74	16.077	41.85	0.28	880	0.8371	1.04	0.1018	0.949	0.93	0.0596	0.386	635	618	591	8.4
INHO13	3	0.015	601.99	65.572	72.55	0.12	851	0.8281	0.98	0.1003	0.85	0.88	0.0598	0.465	616	613	598	10
INHO14	2	0.019	201.34	22.302	57.27	0.28	368	0.8395	2.11	0.1014	1.9	0.91	0.0600	0.864	622	619	606	19

Table 12
Sm–Nd data for the Goianira–Trindade Complex.

Sample	Sm (ppm)	Nd (ppm)	$^{147}Sm/^{144}Nd$	$^{143}Nd/^{144}Nd$	$(^{143}Nd/^{144}Nd)i$	$\varepsilon_{(0)}$	$\varepsilon_{(T)}$	T_{CHUR} (Ma)	T_{DM} (Ma)
GT-4	1.517	4.121	0.223	0.512772	0.511822	2.61	0.43	789	–
GT-6B	3.91	10.68	0.221	0.512748	0.511807	2.15	0.13	703	–
GT-6C	1.663	4.988	0.202	0.512711	0.511850	1.42	0.99	2149	–
GT-9A	2.705	8.329	0.196	0.512648	0.511813	0.20	0.25	–	–
GT-9B	0.881	4.785	0.111	0.5123	0.511827	−6.59	0.53	–	1098
GT-9D	4.833	13.7	0.213	0.512719	0.511812	1.58	0.23	777	–
GT-10B	4.349	12.54	0.21	0.512647	0.511752	0.18	−0.93	–	–
GT-41	0.133	0.463	0.174	0.512704	0.511963	1.29	3.18	–	1281

Table 13
Summary of the main magmatic and tectono-metamorphic episodes of the Neoproterozoic collisional history of the Southern Brasília Belt.

Age	Magmatic/metamorphic events	Temperature regime	References
680–670 Ma	M–UM complexes	Near-peak	This work
	UHT-MP metamorphism (zircon and rutile shielded by garnet)		Möller et al. (2006)
	HP metamorphism (Southern Brasília Belt)		Reno et al. (2009)
	Arc magmatism		(Pimentel et al., 2003a, 2003b; Laux et al., 2005)
650–640 Ma	HT metamorphism (New zircon growth)	Post-peak	(Baldwin and Brown, 2008; Piuzana et al., 2003a)
	D_1 metamorphism (Araxá Group)		D'el-Rey Silva et al. (2004)
	D_2 nappes (Araxá Group)		D'el-Rey Silva et al. (2004)
630–620 Ma	M–UM complexes	Decompressional melting and cooling	(Hollanda et al., 2003; Laux et al., 2004)
	Partial melting (new zircon in leucossomes)		Möller et al. (2006)
	Titanite U–Pb ages (M–UM complexes and UHT granulites)		Moraes et al. (2007)
	Peraluminous granites (AIC)		Piuzana et al. (2003a)
	Pireneus Syntaxis (D_3 folds)		D'el-Rey Silva et al. (2004, 2008)
	Late-orogenic K-rich suite		Pimentel et al. (2003b)

textures, even with the pervasive, although heterogeneous, high-grade metamorphic overprint.

- Whole-rock Sm–Nd isotopic data on the layered complexes reveal a strongly contaminated signature, which indicates that these bodies were emplaced into older continental crust, probably of Paleoproterozoic age.
- CL zircon images reveal internal textures typical of recrystallization, such as irregular, inward-moving boundaries, implying that these crystals were subjected to a varied degree of alteration during high-grade metamorphism.
- Hf-in-zircon analyses yield homogeneous isotopic ratios and ε_{Hf} values (within population), which cannot be linked to the scatter of U–Pb ages, suggesting that the grains were crystallized in one single episode.
- In the studied rocks, during high-grade metamorphism some zircon crystals have re-equilibrated. In these grains, the U–Pb isotopic system was partially reset causing the spread of ages of ca. 80 Ma.
- From the previous statements, it is concluded that the older ages of ca. 670 Ma represent the igneous crystallization of the Damolândia and Taquaral complexes and define an older episode of mafic magmatism in the Brasília Belt than that recorded in the domain of the Goiás Magmatic Arc, to the west. However, the U–Pb data do not allow the discrimination of the peak metamorphic age.
- The data obtained in this study reveals that at least part of the mafic magmatism in the Brasília Belt is coeval with the prograde path of high-grade metamorphism and, therefore, the hot upwelling asthenosphere has promoted partial melting of both mantle and continental crust, generating extensive mafic magmatism and ultrahigh temperature metamorphism.

Acknowledgments

Support from CNPq research grant (477347/2007-0) is thankfully acknowledged. M.M.P. and C.F.F.F. are CNPq research fellows. M.E.S.D. G. thanks CNPq fellowship. The authors are grateful to International Nickel Venture-INV and Amazônia Mineração for providing access to exploration data and support during field work. Horizonte Minerals and BCV Consultoria, which currently hold the mining rights for the Damolândia area, are also acknowledged. Authors would like to thank Renata Schmitt, Claudio Valeriano and Reinhardt A. Fuck for their very useful comments and debates. Two anonymous referees and Karel Schulmann are thanked for careful and constructive reviews on this manuscript. Sérgio Junges, Jeanne Grasyelle and Bárbara Lima are appreciated for providing laboratory assistance.

References

Albarède, F., Telouk, P., Blichert-Toft, J., Boyet, M., Agranier, A., Nelson, B., 2004. Precise and accurate isotopic measurements using multiple collector ICPMS. Geochimica et Cosmochimica Acta 68, 2725–2744.

Ashwal, L.D., Tucker, R.D., Zinner, E.K., 1999. Slow cooling of deep crustal granulites and Pb-loss in zircon. Geochimica et Cosmochimica Acta 63 (18), 2839–2851.

Ayers, J.C., DelaCruz, K., Miller, C., Switzer, O., 2003. Experimental study of zircon coarsening in quartzite $\pm H_2O$ at 1.0 GPa and 1000 °C, with implications for geochronological studies of high-grade metamorphism. American Mineralogist 88, 365–376.

Baldwin, J.A., Brown, M., 2008. Age and duration of ultrahigh-temperature metamorphism in the Anápolis–Itauçu Complex, Southern Brasília Belt, central Brazil — constraints from U–Pb geochronology, mineral rare earth element chemistry and trace element thermometry. Journal of Metamorphic Geology 26, 213–233.

Baldwin, J.A., Powell, R., Brown, M., Moraes, R., Fuck, R.A., 2005. Modelling of mineral equilibra in ultrahigh-temperature metamorphic rocks from the Anápolis–Itauçu Complex, central Brazil. Journal of Metamorphic Geology 23, 511–531.

Bingen, B., Austrheim, H., Whitehouse, M., 2001. Ilmenite as a source for zirconium during high-grade metamorphism? Textural evidence from the Caledonides of western Norway and implications for zircon geochronology. Journal of Petrology 42 (2), 355–375.

Black, L.P., Kamo, S.L., Allen, C.M., Davis, D.W., Aleinikoff, J.N., Valley, J.W., Mundil, R., Campbell, I.H., Korsch, R.J., Williams, I.S., Foudoulis, C., 2004. Improved $^{206}Pb/^{238}U$ microprobe geochronology by the monitoring of a trace-element-related matrix effect; SHRIMP, ID-TIMS, ELA-ICP-MS and oxygen isotope documentation for a series of zircon standards. Chemical Geology 205, 115–140.

Blichert-Toft, J., Chauvel, C., Albarède, F., 1997. Separation of Hf and Lu for high-precision isotope analysis of rock samples by magnetic sector-multiple collector ICPMS. Contributions to Mineralogy and Petrology 127 (3), 248–260.

Brito Neves, B.B., Cordani, U.G., 1991. Tectonic evolution of South America during the late Proterozoic. Precambrian Research 53, 23–40.

Bühn, B., Pimentel, M.M., Matteini, M., Dantas, E.L., 2009. High spatial resolution analysis of Pb and U isotopes for geochronology by laser ablation multi-collector inductively coupled plasma mass spectrometry (LA-MC-ICP-MS). Anais da Academia Brasileira de Ciências 81, 1–16.

Cameron, E.N., 1978. The lower zone of the eastern Bushveld Complex in the Olifants River trough. Journal of Petrology 19, 437–462.

Chu, N.C., Taylor, R.N., Chavagnac, V., Nesbitt, R.W., Boella, R.M., Milton, J.A., German, C.R., Bayon, G., Burton, K., 2002. Hf isotope ratio analysis using multi-collector inductively coupled plasma mass spectrometry: an evaluation of isobaric interference corrections. Journal of Analytical Atomic Spectrometry 17, 1567–1574.

Compston, W., Williams, I.S., Kirschvink, J.L., Zhang, Z.C., Ma, G.G., 1992. Zircon U–Pb ages for the Early Cambrian time-scale. Journal of the Geological Society of London 149, 171–184.

Corfu, F., Hanchar, J.M., Hoskin, P.W.O., Kinny, P., 2003. Atlas of zircon textures. Reviews in Mineralogy and Geochemistry 53, 469–500.

D'el-Rey Silva, L.J.H., Klein, P.B.W., Walde, D.H.G., 2004. The Caldas Novas Dome, Central Brazil: structural evolution and implications for the evolution of Neoproterozoic Brasília Belt. Journal of South American Earth Sciences 17, 153–169.

D'el-Rey Silva, L.J.H., Vasconcelos, M.A.R., Silva, D.V.G., 2008. Timing and role of the Rio Maranhão Thrust in the evolution of the Neoproterozoic Brasília Belt and Tocantins Province, Central Brazil. Gondwana Research 13, 352–374.

Degeling, H., Eggins, S., Ellis, D.J., 2001. Zr budgets for metamorphic reactions, and the formation of zircon from garnet breakdown. Mineralogical Magazine 65 (6), 749–758.

DePaolo, D.J., 1981. A neodymium and strontium isotopic study of the Mesozoic calc-alkaline granitic batholiths of the Sierra Nevada and Peninsular Ranges, California. Journal of Geophysical Research 86, 10470–10488.

Ferreira Filho, C.F., Cançado, F., Correa, C., Macambira, E.M.B., Siepierski, L., Brod, T.C.J., 2007. Mineralizações estratiformes de EGP-Ni associadas a complexos acamadados em Carajás: os exemplos de Luanga e Serra da Onça; in Contribuições à Geologia da Amazônia. Sociedade Brasileira de Geologia — Núcleo Norte 5, 01–14.

Ferreira Filho, C.F., Pimentel, M.M., Araujo, S.M., Laux, J.H., 2010. Layered intrusions and volcanic sequences in Central Brazil: geological and geochronological constraints for Mesoproterozoic (1.25 Ga) and Neoproterozoic (0.79 Ga) igneous associations. Precambrian Research 183 (3), 617–634.

Fraser, G., Ellis, D., Eggins, S., 1997. Zirconium abundance in granulite-facies minerals, with implications for zircon geochronology in high-grade rocks. Geology 25, 607–610.

Fuck, R.A., Pimentel, M.M., Silva, L.J.H.D., 1994. Compartimentação tectônica da porção oriental da Província Tocantins. 38th Congresso Brasileiro de Geologia, Anais, vol. 1, pp. 215–216.

Geisler, T., Schaltegger, U., Tomaschek, F., 2007. Re-equilibration of zircon in aqueous fluids and melts. Elements 3, 43–50.

Gerdes, A., Zeh, A., 2009. Zircon formation versus zircon alteration — new insights from combined U–Pb and Lu–Hf in-situ LA-ICP-MS analyses, and consequences for the interpretation of Archean zircon from the Central Zone of the Limpopo Belt. Chemical Geology 261, 230–243.

Gioia, S.M., Pimentel, M.M., 2000. The Sm–Nd isotopic method in the geochronology laboratory of the University of Brasília. Anais da Academia Brasileira de Ciências 72 (2), 219–254.

Giustina, M.E.S.D., Oliveira, C.G., Pimentel, M.M., Buhn, B., 2009. Neoproterozoic magmatism and high-grade metamorphism in the Goiás Massif: new LA-MC-ICMPS U–Pb and Sm–Nd data and implications for collisional history of the Brasília Belt. Precambrian Research 172, 67–79.

Harley, S.L., 1998. On the occurrence and characterization of ultrahigh-temperature crustal metamorphism. Geological Society of London. Special Publication 138, 81–107.

Harley, S.L., 2004. Extending our understanding of ultrahigh temperature crustal metamorphism. Journal of Mineralogical and Petrological Sciences 99, 140–158.

Harley, S.L., 2008. Refining the P–T records of UHT crustal metamorphism. Journal of Metamorphic Geology 26, 125–154.

Hollanda, M.H.B.M., Pimentel, M.M., Armstrong, R., 2003. Isotopic and geochronological constraints for the origin of syn- to post-Brasiliano mafic magmatism and crustal re-melting in the Brasília Belt (Central Brazil). IV SSAGI, Salvador, pp. 194–197 (Short Papers).

Hoskin, P.W., Black, L.P., 2000. Metamorphic zircon formation by solid-state recrystallization of protolith igneous zircon. Journal of Metamorphic Geology 18, 423–439.

Jackson, S.E., Pearson, N.J., Griffin, W.L., Belousova, E.A., 2004. The application of laser ablation-inductively coupled plasma-mass spectrometry to in situ U–Pb zircon geochronology. Chemical Geology 211, 47–69.

Kelly, N.M., Harley, S.L., 2005. An integrated microtextural and chemical approach to zircon geochronology: refining the Archaean history of the Napier Complex, east Antarctica. Contributions to Mineralogy and Petrology 149, 57–84.

Krogh, T.E., 1973. A low-contamination method for hydrothermal decomposition of zircon and extraction of U and Pb for isotopic age determinations. Geochimica et Cosmochimica Acta 37, 485–494.

Laux, J.H., Pimentel, M.M., Dantas, E.L., Armstrong, A., Armele, R., Nilson, A.A., 2004. Mafic magmatism associated with the Goiás magmatic arc in the Anicuns region, Goiás, central Brazil central Brazil: Sm–Nd isotopes and new ID-TIMS and SHIMP U–Pb data. Journal of South American Earth Sciences 16, 599–614.

Laux, J.H., Pimentel, M.M., Dantas, E.L., Armstrong, R., Junges, S.L., 2005. Two Neoproterozoic crustal accretion events in the Brasília Belt, Central Brazil. Journal of South American Earth Sciences 18, 183–198.

Ludwig, K.R., 1993. PBDAT. A computer program for processing Pb–U–Th isotope data. USGS Open File Report, vol. 88–542, p. 34.

Ludwig, K.R., 2001. Squid 1.02. A User's Manual: BGC Special Publication, vol. 2. Berkeley, 19 pp.

Ludwig, K.R., 2003. User's Manual for Isoplot/Ex v. 3.00. A Geochronological Toolkit for Microsoft Excel: BGC Special Publication, vol. 4. Berkeley, 71 pp.

Martin, L.A., Duchene, S., Deloule, E., Vanderhaeghe, O., 2008. Mobility of trace elements and oxygen in zircon during metamorphism: consequences for geochemical tracing. Earth and Planetary Science Letters 267, 161–174.

Matteini, M., Junges, S.L., Dantas, E.L., Pimentel, M.M., Buhn, B., 2010. In situ zircon U–Pb and Lu–Hf isotope systematic on magmatic rocks: insights on the crustal evolution of the Neoproterozoic Goiás Magmatic Arc, Brasília belt, Central Brazil. Gondwana Research 17 (1), 1–12.

Mezger, K., Krogstad, E.J., 1997. Interpretation of discordant U–Pb ages. An evaluation. Journal of Metamorphic Geology 15, 127–140.

Möller, A., O'Brien, P.J., Kennedy, A., Kroner, A., 2002. Polyphase zircon in ultrahigh-temperature granulites (Rogaland, SW Norway): constraints for Pb diffusion in zircon. Journal of Metamorphic Geology 20, 727–740.

Möller, A., O'Brien, P.J., Kennedy, A., Kröner, A., 2003. Linking growth episodes of zircon and metamorphic textures to zircon chemistry: an example from the ultrahigh-temperature granulites of Rogaland (SW Norway). Geological Society of London. Special Publication 220, 65–81.

Möller, A., Moraes, R., Hellebrand, E., Kennedy, A., Fuck, R.A., 2006. Age and duration of the UHT Event in the Brasilia Fold Belt: in-situ dating of zircon and rutile and equilibrium REE distribution between zircon and orthopyroxene. Granulites & Granulites, p. 54. Brasilia.

Moraes, R., Brown, M., Fuck, R.A., Camargo, M.A., Lima, T.M., 2002. Characterization and P–T evolution of melt-bearing ultrahigh-temperature granulites: an example from the Anápolis–Itauçu Complex of the Brasília Fold Belt, Brazil. Journal of Petrology 43 (9), 1673–1705.

Moraes, R., Fuck, R.A., Brown, M., Piccoli, P., Baldwin, J., Dantas, E.L., Laux, J.H., Junges, S., 2007. Wollastonite–scapolite–clinopyroxene marble of the Anápolis–Itauçu Complex, Goiás: more evidence of ultrahigh-temperature metamorphism. Revista Brasileira de Geociencias 37 (4), 11–17.

Morel, M.L., Nebel, O., Nebel-Jacobsen, Y.J., Miller, J.S., Vroon, P.Z., 2008. Hf isotope characterization of the GJ-1 zircon reference material by solution and laser-ablation MC-ICPMS. Chemical Geology 255, 231–235.

Nebel, O., Nebel-Jacobsen, Y., Mezger, K., Berndt, J., 2007. Initial Hf isotope compositions in magmatic zircon from early Proterozoic rocks from the Gawler Craton, Australia: a test for zircon model ages. Chemical Geology 241, 23–37.

Nilson, A.A., 1992. Geologia e aspectos petrológicos do complexo máfico–ultramáfico de Águas Claras, Araçu, Goiás. XXXVII Congresso Brasileiro de Geologia, p. 457. São Paulo.

Nilson, A.A., Motta, F., 1969. Geologia da área de Goianira–Trindade. DNPM, Bol. Div. Fom. Da Produção Mineral, vol. 133. 108 pp.

Nystrom, A.I., Kriegsman, L.M., 2003. Prograde and retrograde reactions, garnet zoning patterns, and accessory phase behaviour in SW Finland migmatites, with implications for geochronology. In: VANCE, D., MOLLER, W., VILLA, I.M. (Eds.), Geochronology: Linking the Isotopic Record with Petrology and Textures: Geological Society London, Special Publications, vol. 220, pp. 213–230.

Paces, J.B., Miller, J.D., 1993. Precise U–Pb ages of Duluth Complex and related mafic intrusions, northeastern Minnesota: geochronological insights to physical, petrogenetic, paleomagnetic and tectonomagmatic processes associated with the 1.1 Ga mid-continent rift system. Journal of Geophysical Research 98, 13997–14013.

Pimentel, M.M., Fuck, R.A., 1992. Neoproterozoic crustal accretion in central Brazil. Geology 20, 375–379.

Pimentel, M.M., Fuck, R.A., Jost, H., Ferreira Filho, C.F., Araújo, S.M., 2000. The basement of the Brasília Fold Belt and the Goiás Magmatic Arc. In: Cordani, U.G., Milani, E.J., Thomaz Filho, A., Campos, D.A. (Eds.), The Tectonic Evolution of South America, Rio de Janeiro: Proceedings of the 31st International Geological Congress, pp. 195–229.

Pimentel, M.M., Dantas, E.L., Fuck, R.A., Armstrong, R., 2003a. SHRIMP and conventional U–Pb age, Sm–Nd characteristics and tectonic significance of K-rick Itapuranga suite in Goiás, Central Brazil. Anais da Academia Brasileira de Ciências 75 (1), 97–108.

Pimentel, M.M., Laux, J.H., Hollanda, M.H.B.M., Gioia, S.M.C.L., 2003b. The Brasília Belt as a "Hot Orogen": new SHRIMP and conventional U–Pb data and Sm–Nd isotopic constraints from terminal mafic magmatism in central-western Goiás. III International Symp. on Tectonics, pp. 21–23. Búzios.

Piuzana, D., Pimentel, M.M., Fuck, R.A., Armstrong, R., 2003a. Neoproterozoic granulite facies metamorphism and coeval granitic magmatism in the Brasilia Belt, Central Brazil: regional implications of new SHRIMP U–Pb and Sm–Nd data. Precambrian Research 125, 245–273.

Piuzana, D., Pimentel, M.M., Fuck, R.A., Armstrong, R., 2003b. SHRIMP U–Pb and Sm–Nd data for the Araxá Group and associated magmatic rocks: constraints for the age of sedimentation and geodynamic context of the southern Brasília Belt, central Brazil. Precambrian Research 125, 139–160.

Putnis, A., 2002. Mineral replacement reactions: from macroscopic observations to microscopic mechanisms. Mineralogical Magazine 66 (5), 689–708.

Reno, B.L., Brown, M., Kobayashi, K., Nakamura, E., Piccoli, P.M., Trowu, R.A.J., 2009. Eclogite-high-pressure granulite metamorphism records early collision in West Gondwana: new data from the Southern Brasília Belt, Brazil. Journal of the Geological Society 166, 1013–1032.

Roberts, M.P., Finger, F., 1997. Do U–Pb zircon ages from granulites reflect peak metamorphic conditions? Geology 25, 319–322.

Rubatto, D., 2002. Zircon trace element geochemistry: partitioning with garnet and the link between U–Pb ages and metamorphism. Chemical Geology 184, 123–138.

Rubatto, D., Hermann, J., 2007. Experimental zircon / melt and zircon / garnet trace element partitioning and implications for the geochronology of crustal rocks. Chemical Geology 241, 38–61.

Schaltegger, U., Fanning, M., Günther, D., Maurin, J.C., Schulmann, K., Gebauer, D., 1999. Growth, annealing and recrystallization of zircon and preservation of monazite in high-grade metamorphism: conventional and in-situ U–Pb isotope, cathodoluminescence and microchemical evidence. Contributions to Mineralogy and Petrology 134, 186–201.

Silva, F.O., 1991. Geologia, estrutura, petrologia e mineralização de Fe, Ti e V associadas ao complexo gabro-anortosítico acamadado de Santa Bárbara (Goiás). Dissertação de Mestrado, Universidade de Brasília, 190 pp.

Silva, F.O., 1997. Geologia e petrologia do extremo noroeste do Complexo máfico–ultramáfico de Taquaral, GO. Tese de Doutorado, Universidade de Brasília, 171 pp.

Sláma, J., Kosler, J., Pedersen, R.B., 2007. Behaviour of zircon in high-grade metamorphic rocks: evidence from Hf isotopes, trace elements and textural studies. Contributions to Mineralogy and Petrology 154, 335–356.

Tomaschek, F., Kennedy, A.K., Villa, I.M., Lagos, M., Ballhaus, C., 2003. Zircons from Syros, Cyclades, Greece: recrystallization and mobilization of zircon during high-pressure metamorphism. Journal of Petrology 44 (11), 1977–2002.

Valeriano, C.M., Pimentel, M.M., Heilbron, M., Almeida, J.C.H., Trouw, R.A.J., 2008. Tectonic evolution of the Brasília Belt, Central Brazil, and early assembly of Gondwana. In: Pankhurst, R.J., Trouw, R.A.J., Brito Neves, B.B., de Wit, M.J. (Eds.), West Gondwana: Prec-Cenozoic Correlations Across the South Atlantic Region: Geological Society of London, Special Publications, vol. 294, pp. 197–210.

Vavra, G., Schmid, R., Gebauer, D., 1999. Internal morphology, habit and U–Th–Pb microanalysis of amphibolite-to-granulite facies zircons: geochronology of the Ivrea Zone (Southern Alps). Contributions to Mineralogy and Petrology 134, 380–404.

Whitehouse, M.J., Platt, J.P., 2003. Dating high-grade metamorphism-constraints from rare-earth elements in zircon and garnet. Contributions to Mineralogy and Petrology 145, 61–74.

Williams, I.S., Claesson, S., 1987. Isotopic evidence for the Pre-Cambrian provenance and Caledonian metamorphism of high grade paragneisses from the Svecoffenian Nappes, Scandinavia Caledonides: II Ion microprobe zircon U–Th–Pb. Contributions to Mineralogy and Petrology 97, 205–217.

Wilson, A.H., 1982. The geology of the Great 'Dyke', Zimbabwe: the ultramafic rocks. Journal of Petrology 23, 240–292.

Winge, M., 1995. Evolução dos terrenos granulíticos da Província Tocantins, Brasil Central. Tese de Doutorado, Universidade de Brasília, 550 pp.

Winge, M., Danni, J.C.M., 1994. Gênese de sillimanita granada leptinitos no Complexo Anápolis–Itauçu,Goiás. Congresso Brasileiro de Geologia, 38, Camboriú-SC, 1994, SBG: Boletim de Resumos Expandidos, vol. 2, pp. 76–77.

Xia, Q.X., Zheng, Y.F., Yuan, H., Wu, F.Y., 2009. Contrasting Lu–Hf and U–Th–Pb isotope systematic between metamorphic growth and recrystallization of zircon from eclogite-facies metagranites in the Dabie orogen, China. Lithos 112, 477–496.

Xie, L.W., Zhang, Y.B., Zhang, H.H., Sun, J.F., Wu, F.Y., 2008. In situ simultaneous determination of trace elements, U–Pb and Lu–Hf isotopesin zircon and baddeleyite. Chinese Science Bulletin 53 (10), 1565–1573.

Zack, T., Luvizotto, G.L., Moraes, R., Möller, A., Kronz, A., 2006. Rutile and zircon thermometry of granulites: premetamorphic relicts, prograde growth, disequilibrium and diffusional resetting. Granulites & Granulites, p. 98. Brasilia.

Zeh, A., Gerdes, A., Klemd, R., Barton Jr., J.M., 2007. Archaean to Proterozoic crustal evolution in the central zone of the Limpopo Belt (South Africa–Botswana): constraints from combined U–Pb and Lu–Hf isotope analyses of zircon. Journal of Petrology 48 (8), 1605–1639.